Reconciling onshore and offshore geological mapping: lessons from north Cornwall, SW England

Benjamin Craven* and Geoffrey E. Lloyd

School of Earth and Environment, The University of Leeds, Leeds LS2 9JT, UK

BC, 0000-0002-9290-8723; GEL, 0000-0002-7859-2486

*Correspondence: B.Craven@leeds.ac.uk

Abstract: We present the first detailed stratigraphic and structural geological map of offshore north Cornwall and Devon, SW England, based on freely available bathymetric data. Although the bathymetry is often spectacular, revealing fold and fault structures exposed on the seabed at a range of scales and with high resolution, interpretation is not as straightforward as it might appear and depends critically upon both accuracy and knowledge of the onshore geology. Unfortunately, onshore stratigraphic controls are limited and restricted to several thin 'named shales' whose coastal outcrops are not always well constrained. In addition, the structure is markedly non-cylindrical on local to regional scales, making seaward projection problematic, while the impact of early thrusting on the stratigraphy has often been previously neglected. We therefore developed a workflow to handle the problems we encountered, including: recognition of vertical to horizontal and 3D to 2D projections; variations in bathymetric data characteristics; prediction of expected seabed outcrop geometries based on coastal structures; incorporation of non-cylindrical effects; and problems with quantitative GIS terrain profiles and structural measurements that result in an absence of such measurements. The geological map produced should therefore be viewed as a step forward, but as forming a base for further detailed bathymetric mapping.

Geological mapping is historically and conventionally land-based, with map data collected from observations made at outcrop scale. More recently, remote sensing mapping has become widely established, using high-resolution techniques such as aerial photography (www.channelcoast.org), InSAR (Burgmann *et al.* 2000), LiDAR (Cracknell and Hayes 2007), infra-red (Roy *et al.* 2009), seismic (Virtual Seismic Atlas, www.seismicatlas.org and geochemistry (Tellus Southwest, https://mapapps2.bgs.ac.uk/tellussw/home.html). Remote sensing allows mapping of isolated and/or inaccessible areas and is becoming increasingly important to meet many modern and future societal demands such as offshore engineering, oil, gas and renewable resources. One particular remote sensing process applied to effectively inaccessible regions is bathymetry: mapping variations in the depth of a body of water. As technology develops and societal demands advance, it is becoming increasingly important to extend geological maps and interpretations offshore, particularly on the continental shelf. Furthermore, detailed geological mapping is usually restricted to onshore outcrop which can lead to problems with understanding and controversy of interpretation. Extending geological maps offshore could therefore provide increased understanding and further insights. Thus it is not surprising that high-resolution bathymetric surveys are being used as a basis for geological mapping, for example by Nixon *et al.* (2012) and the British Geological Survey (BGS) Geoindex Offshore (https://mapapps2.bgs.ac.uk/geoindex_offshore/home.html?_ga=2.93081885.1476607356.1670326362-406467234.1670326362) resources. However, unfortunately interpreting these surveys geologically is not always as easy as it may at first appear, as we demonstrate here.

Nixon *et al.* (2012) have previously reported a bathymetry study of the offshore region to the north and west of Hartland Point at the northern end of our study area (Fig. 1b). Their study revealed a submerged platform of bedrock extending *c.* 2.5 km from the shoreline that provided a much more extensive area (*c.* 16 km^2) than that exposed at low tide on the wave-cut platform. They argued that the bathymetric data allowed direct correlation of bedding and faults with features mapped onshore on the platforms. However, in practice, their correlations generally relied on locations where the bathymetry and land images actually intersected, which is not usually the case (e.g. owing to water depth preventing surveying close to the shoreline and/or proximal sand bodies). We show in this contribution that several factors can lead to significant problems with the extrapolation of the known geology where onshore data must be extrapolated to reach the offshore bathymetric data. In addition, Yeomans *et al.* (2021) have recently shown how semi-automated lineament detection methods can be applied to high-resolution bathymetry surveys, again from offshore

From: Butler, R. W. H., Torvela, T. and Williams, L. (eds) *Geological Mapping of Our World and Others.* Geological Society, London, Special Publications, **541**,
https://doi.org/10.1144/SP541-2022-314

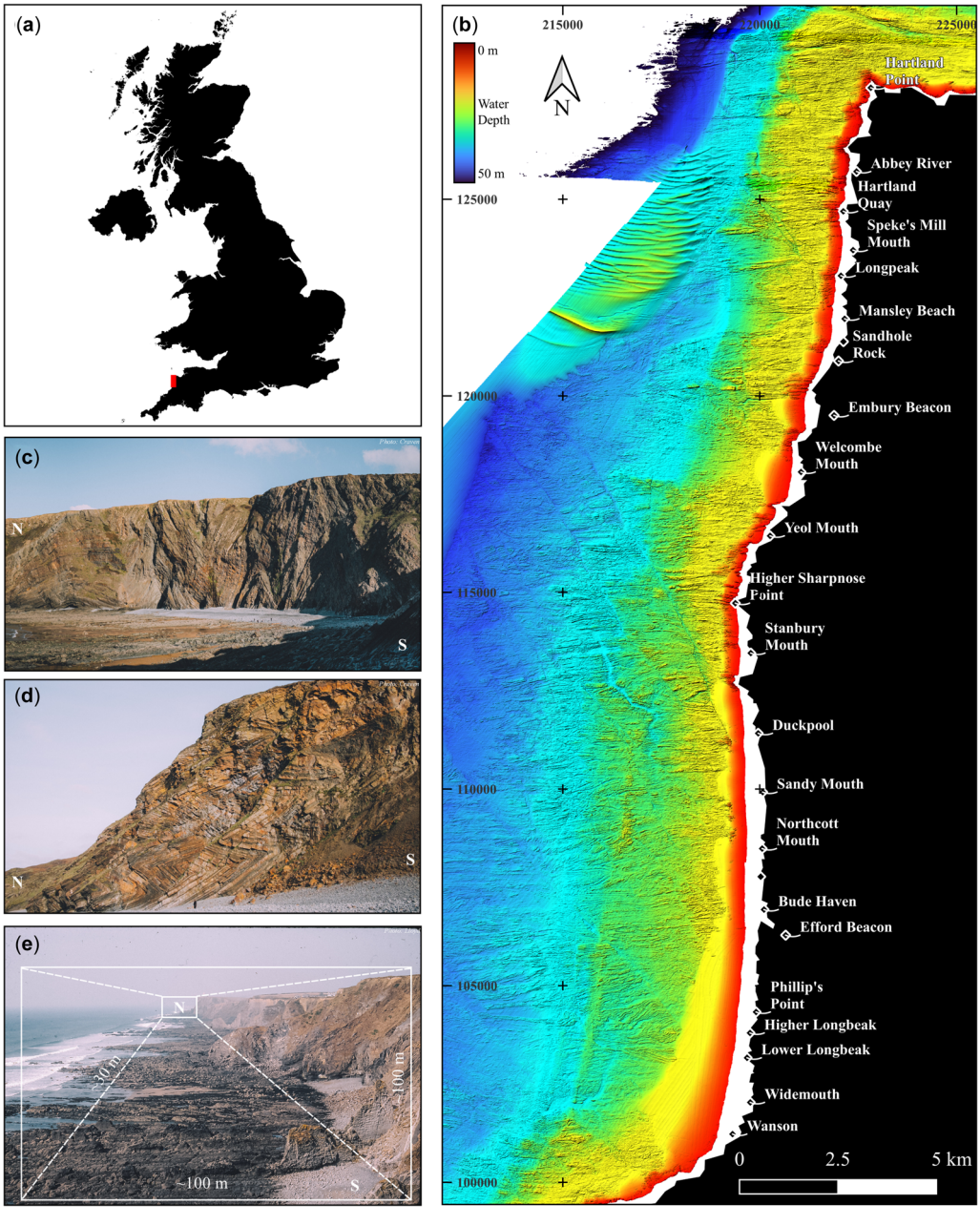

Fig. 1. (**a**) General location of study area. (**b**) Bathymetry (hillshade overlying single-band pseudo-colour) of study area. (**c**) Vertical chevron folds, Hartland Quay (cliffs *c.* 90 m high). (**d**) Recumbent chevron folds, Millook Haven (cliffs *c.* 80 m high). (**e**) General view northwards of north Cornish coastline from north Widemouth Bay; note 'rectangular parallelepiped' nature of the outcrop section.

north Cornwall and Devon, to identify lineaments in a range of orientations and across sharp steps in the seafloor topography. Conclusions using this technique could be enhanced by combining them with the seafloor geology.

This contribution describes the use of bathymetry to extrapolate the well-exposed but limited coastal geology of north Cornwall and Devon, SW England (Fig. 1a), for up to *c.* 10 km offshore to the west (Fig. 1b). This coastline is justifiably famous for its

Upper Carboniferous sedimentary succession (e.g. Macintosh 1964; Lovell 1965; Freshney *et al.* 1972, 1979; Freshney and Taylor 1972; Melvin 1986; Thomas 1988; Hartley 1991, 1993; Higgs 1991) and Variscan structural geology (e.g. Dearman 1969; Freshney *et al.* 1972, 1979; Sanderson and Dearman 1973; Ramsay 1974; Sanderson 1974, 1979; Hobson and Sanderson 1975; Ferguson and Lloyd 1982; Rattey and Sanderson 1982; Enfield *et al.* 1985; Selwood *et al.* 1985; Lloyd and Whalley 1986, 1997; Whalley and Lloyd 1986; Thompson and Cosgrove 1996 and references therein; Thomas 1988; Tanner 1989, 1992; Warr 1989, 2012; Mapeo and Andrews 1991; Lloyd and Chinnery 2002; Davison *et al.* 2004).

The effectively continuously exposed coastal outcrops provide a regional structural cross-section extending for almost 30 km between Hartland Point in the North (Fig. 1c) and Millook Haven in the South (Fig. 1d). However, the apparently excellent exposure masks a problem that impacts significantly on geological interpretation. In practice, exposure is limited to up to 200 m wide wavecut platforms, which provide continuous 'map-views', and up to 150 m high cliff profiles, which provide continuous 'cross-sectional views'. Thus, three-dimensional visualization of the geology is effectively restricted to a maximum 200 m × 150 m × 30 km 'rectangular parallelepiped' (Fig. 1e). Nevertheless, the excellent continuous although spatially restricted coastal outcrop exposures of north Cornwall and Devon enable the construction of detailed regional geological cross-sections (e.g. King 1967; Freshney *et al.* 1972, 1979; Lloyd and Chinnery 2002; Davison *et al.* 2004).

In this contribution, we consider the extrapolation of the known land geology of north Cornwall and Devon westwards beneath the sea via the interpretation of bathymetric data. We show that in spite of the generally excellent bathymetric surveys, supported by equally excellent coastal aerial photograph images and LiDAR data, extrapolation is not as straightforward as it might first seem. We therefore also focus on explaining the challenges encountered, developing workflows that can be followed to eventually produce a map based on the interpretation of the bathymetric data. We begin by explaining our approach to the bathymetric mapping and related techniques involved, including definition of the currently accepted geological framework and consideration of the three-dimensional visualization of the known structural geology on land and its projection onto a two-dimensional seabed. We argue that this 3D to 2D projection is crucial for valid extrapolation and the production of an offshore geological map. Finally, we discuss in more detail the geological problems recognized during the construction of our final map and suggest how this may be improved if more geological data, especially stratigraphic, became available.

Methods

The principal aim of this contribution is to investigate the procedures involved in the construction of a bathymetry-based geological map of the seabed, offshore north Cornwall and Devon. The result is not just a geological map, but also a baseline workflow model to aid construction of such maps that recognizes the potential pitfalls that exist in extrapolating onshore geology further offshore. In this respect, we have combined bathymetric data with available field and aerial photography and LiDAR data within a common GIS environment.

Bathymetry

While topography shows elevation of landforms above sea-level, bathymetry shows depths of landforms below sea-level. Bathymetric surveys measure the depth to the seabed from point to point based on the speed of sound in water as a function of depth (i.e. sound-speed profiles) after correcting refraction effects owing to the temperature, conductivity, and pressure of the water column (e.g. Finkl and Makowski 2016). The smaller the individual beam aperture, the smaller the footprint and the higher the resolution. Modern multibeam echosounders can adjust the swath (i.e. angular distance between beams) but as the individual beams retain fixed apertures and footprints, which are the limiting factors for horizontal resolution, the resolution of a bathymetric dataset will often decrease with increasing water depth.

High-resolution multibeam bathymetry datasets of the seabed, offshore north Cornwall, were acquired via UK Admiralty Surveys between 2008 and 2011 as part of the UK Civil Hydrography Programme (UK Hydrographic Office data © Crown copyright and database multibeam bathymetry data HI 1158, Barnstaple Bay Part 2, and HI 1157, Hartland Point to Land's End Blk1, under Bathymetry Data License v.1; https://data.admiralty.co.uk/portal/apps/sites/#/marine-data-portal). Surveying was able to access water depths as low as *c.* 1 m chart datum. The bathymetry datasets were imported into QGIS, a free and open source geographical information system application (qgis.osgeo.org), which was used to produce geo-referenced images with 2 m horizontal resolution. Images were examined via several rendering methods, which convert geometry, colouring, texturing, lighting and other characteristics of an object into a visual display. Rendering methods include: *Hillshade* (e.g. Fig. 2a), which creates a hill shade effect depending on a

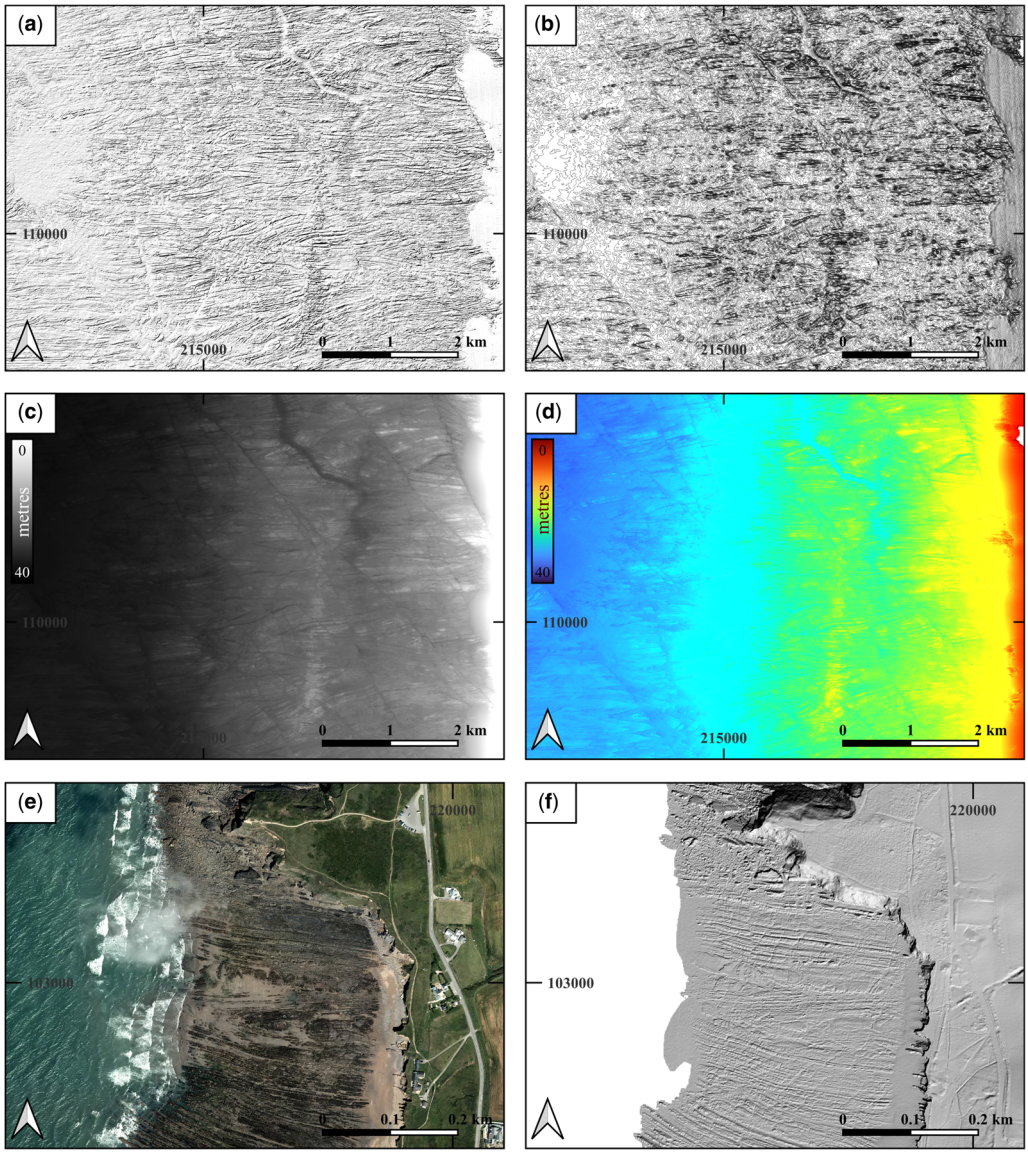

Fig. 2. (**a**)–(**e**) Examples of types visual processing of bathymetric data, north Cornwall. (**a**) Hillshade ('sun' azimuth 45° from north). (**b**) Contours (0.2 m intervals). (**c**) Single-band grey (relative elevations); note image exceeding scaling limits left (minimum) and right (maximum). (**d**) Single-band pseudocolour (red, shallowest). (**e**) and (**f**) Aerial photograph and LiDAR ('sun' azimuth 45° from south) images of coastline, north Cornwall.

chosen plunge and azimuth of sunlight; *Contours* (e.g. Fig. 2b), a conventional map of topographic highs and lows; *Single-band grey* (e.g. Fig. 2c), where one the data bands of the image is rendered in conventional greyscale between defined minimum and maximum values; and *Single-band pseudocolour* (e.g. Fig. 2d), where that data band is assigned a range of colours defined by the user. *Hillshade* is conventionally used to accentuate features such as bedding and fault traces, from which offsets of marker beds and displacements can be measured, as well as slopes and hence the strike and dip of identified bedding planes (e.g. Nixon *et al.* 2012). However, we found that such images were not always ideal as the relative depth of a feature is often just as important: compare Figure 2a and c. We therefore used different methods, or a combination of methods, where appropriate

Aerial photography

In addition to, and to provide continuity with, the onshore geology, we have also made use of high-resolution aerial photography images of the adjacent coastline obtained from the Channel Coastal Observatory (https://coastalmonitoring.org/). They provide not only a direct link to the natural landscape, but also permit visual inspection of localities that are difficult to access – a particular problem in the north of the study area.

LiDAR

LiDAR (light detection and ranging) data augment the aerial photograph images of the coastline (e.g. Fig. 2f). The LiDAR data, which were also obtained from the Channel Coast Observatory, provide high-resolution models of ground elevation and as such create an image somewhat equivalent to that obtained via bathymetry. Indeed, similar rendering methods are employed.

Field observations

In general, the structure of north Cornwall and Devon is apparently simple and dominated by ~east–west-trending upright to overturned chevron folds, seen in Figure 1c and d, historically considered to form the so-called 'Culm Synclinorium' (Ussher 1892). A 'supracrustal-infracrustal' model is also often adopted (e.g. Zwart 1964), in which the Upper Carboniferous rocks 'crumpled' above a basal detachment that (probably) crops out to the south as the Rusey Fault Zone (e.g. Owen 1934; Freshney *et al.* 1972; Ferguson and Lloyd 1982; Thompson and Cosgrove 1996) and subsea to the north in the Bristol Channel (e.g. Le Gall 1990, 1991).

The lithologies along the coastline are typically alternating sandstones and shales with occasional conspicuous slump beds of the Upper Carboniferous Crackington and Bude Formations (Fig. 3). Together they present a monotonous sequence with few distinctive marker horizons. In general, sandstones are thinner in the Crackington Formation, while the Bude Formation contains more sandstone than shale. Lithologies are therefore similar throughout. Both formations are typically unfossiliferous and few control fossils are present (e.g. Freshney *et al.* 1972, 1979). Those that do occur are rare and restricted to several 'named shale' horizons, although not all occurrences of these shales contain the diagnostic fauna (Fig. 3). Indeed, the whole of the >1200 m thick Bude Formation is effectively barren apart from the Hartland Quay Shale (*Gastrioceras amaliae*) immediately beneath its base, the Sandy Mouth Shale (*Anthracoceratoides cornubiensis* Ramsbottom) in its centre and the Warren Gutter Shale (*Donetzoceras aegiranum* Schmidt) beneath its observed upper extent. The lower half of the formation relies on recognition and/or distinction between three slump bed horizons (Church Races, Black Rock and Phillip's). In contrast, the <400 m of observed Crackington Formation has three 'named' shales defined by zonal fossils (Fig. 3): Embury Shale (*Gastrioceras subcrenatum*), Gull Rock Shale (*Gastrioceras listeri*) and Hartland Quay Shale (*Gastrioceras amaliae*).

The classic structural interpretation follows the standard stratigraphy (Fig. 3) and favours a continuous north–south sequence of upright-to-inclined chevron folds (e.g. Dearman 1969; Freshney *et al.* 1972, 1979; Sanderson and Dearman 1973; Ramsay 1974; Sanderson 1974, 1979; Hobson and Sanderson 1975). We have chosen to use the British Geological Survey cross-sections combined from the relevant published map sheets (292 Bideford and Lundy, 307–308 Bude and 322 Boscastle), which form a coherent structural profile (Fig. 4). The combined section was constructed by tracing a stratigraphy defined by 'named shales' and slump bed horizons within the Crackington and Bude Formations. The BGS section provides a basic framework from which to extrapolate specific aspects of the on-shore geology offshore into the bathymetric data. In particular, the localities given by the BGS (Freshney *et al.* 1972, 1979) for the 'named shales' (Figs 3 & 4) represent tight but limited local constraints that can be projected seawards.

Workflow: GIS Bathymetric Mapping

The bathymetry, aerial photography and LiDAR data were combined into a single project using QGIS. However, before the model could be interrogated to produce a seabed geological map, several preliminary geometrical and structural aspects need to be considered, as follows.

Seabed topography

It is first necessary to define the basic topography of the seabed relative to the individual geological features. Reconnaissance of the seabed offshore north Cornwall in QGIS indicates that after an initial relative steep slope over *c.* 2 km from the shoreline, it becomes essentially planar with a very gentle slope for up to the next *c.* 20 km (Fig. 5a). However, the slope is steeper and the outcrop narrower in the north around Hartland. Any local topography is usually of the order of a few metres and so does not affect the perception of the stratal geometry in a significant way.

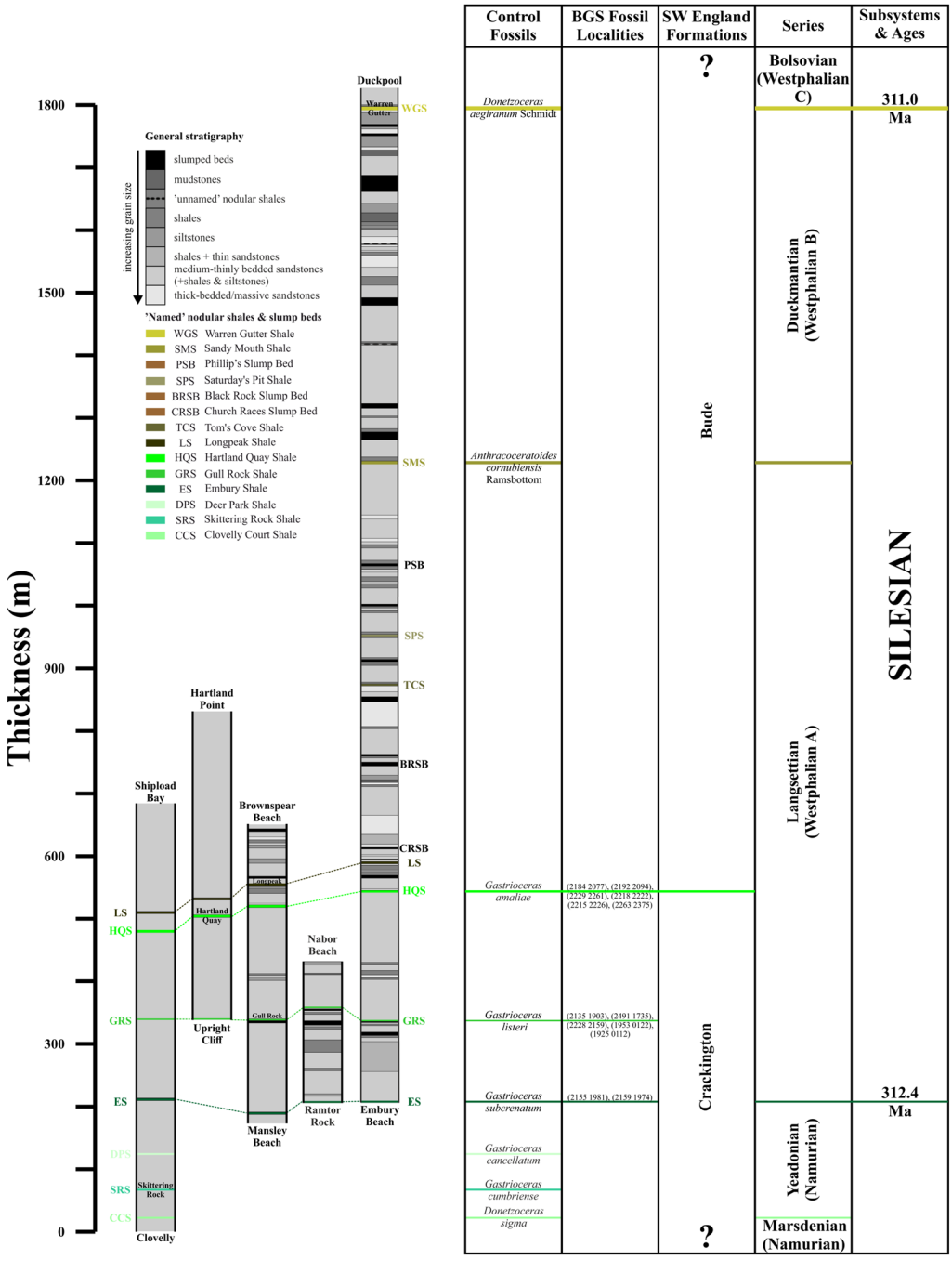

Fig. 3. Upper Carboniferous stratigraphy: fossiliferous marine bands and 'named' shales and slump beds in north Cornwall, extending from the Embury Shale to the Warren Gutter Shale; older shales are not exposed along the coastal section but maybe offshore. Source: Figure compiled from: King (1967); Freshney and Taylor (1972), Freshney *et al.* (1979), Cleal and Thomas (1996) and Rippon (1996). Ages from Hess and Lippolt (1986) and Claoue-Long *et al.* (1993).

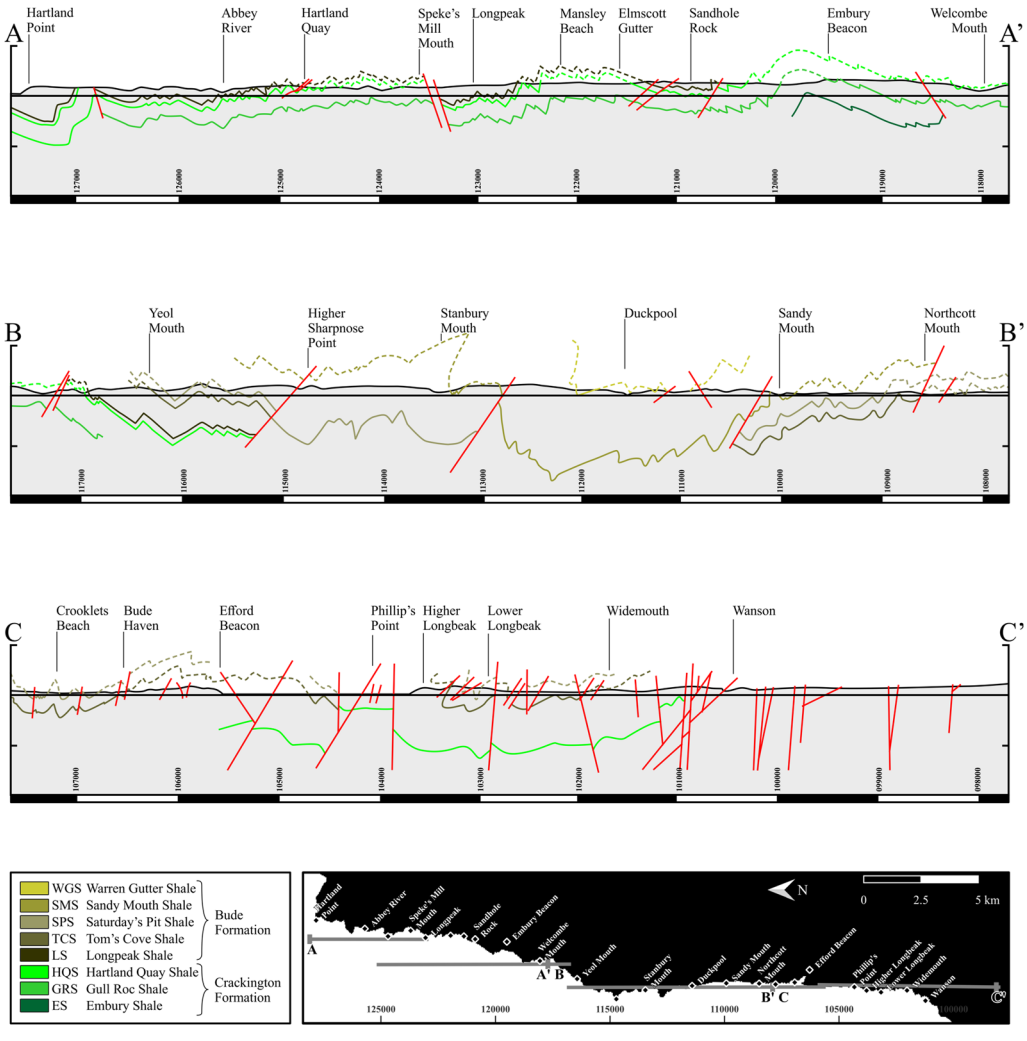

Fig. 4. Compilation of British Geological Survey cross-sections (sheets 292 Bideford and Lundy, 307–308 Bude and 322 Boscastle) to produce a continuous section from Hartland Point to the Rusey Fault Zone south of Millook Haven.

Most of the seabed appears to be clear of surficial sediments, such that the bedrock is often fully exposed (Fig. 5b). However, sand bodies do occur and can completely obscure the bedrock beneath. Most of these bodies extend seawards from the coastline for up to *c.* 1 km, although two much larger bodies occur further offshore (Fig. 5c). The latter are characterized by bedforms on their upper surfaces (Fig. 5d) and channels on their sides (Fig. 5e). In addition, suspended sediment occurs intermittently and acts to obscure the bedrock depending on its concentration (Fig. 5e). Indeed, several meandering channels can be observed, filled with sand that noticeably thins distally (Fig. 5g).

Vertical-to-horizontal projection: basic considerations

The next step is to consider the projection of features observed in the cliff profile section (e.g. Fig. 4) onto the wavecut platform and seabed. Depending on the degree of structural plunge, features project with varying obliquity onto the gently inclined surfaces, resulting in distortion parallel to the plunge azimuth. The sense and magnitude of the distortion (d) depends on the tangent of the plunge (ϕ),

$$d = h/\tan(\phi) \quad (1)$$

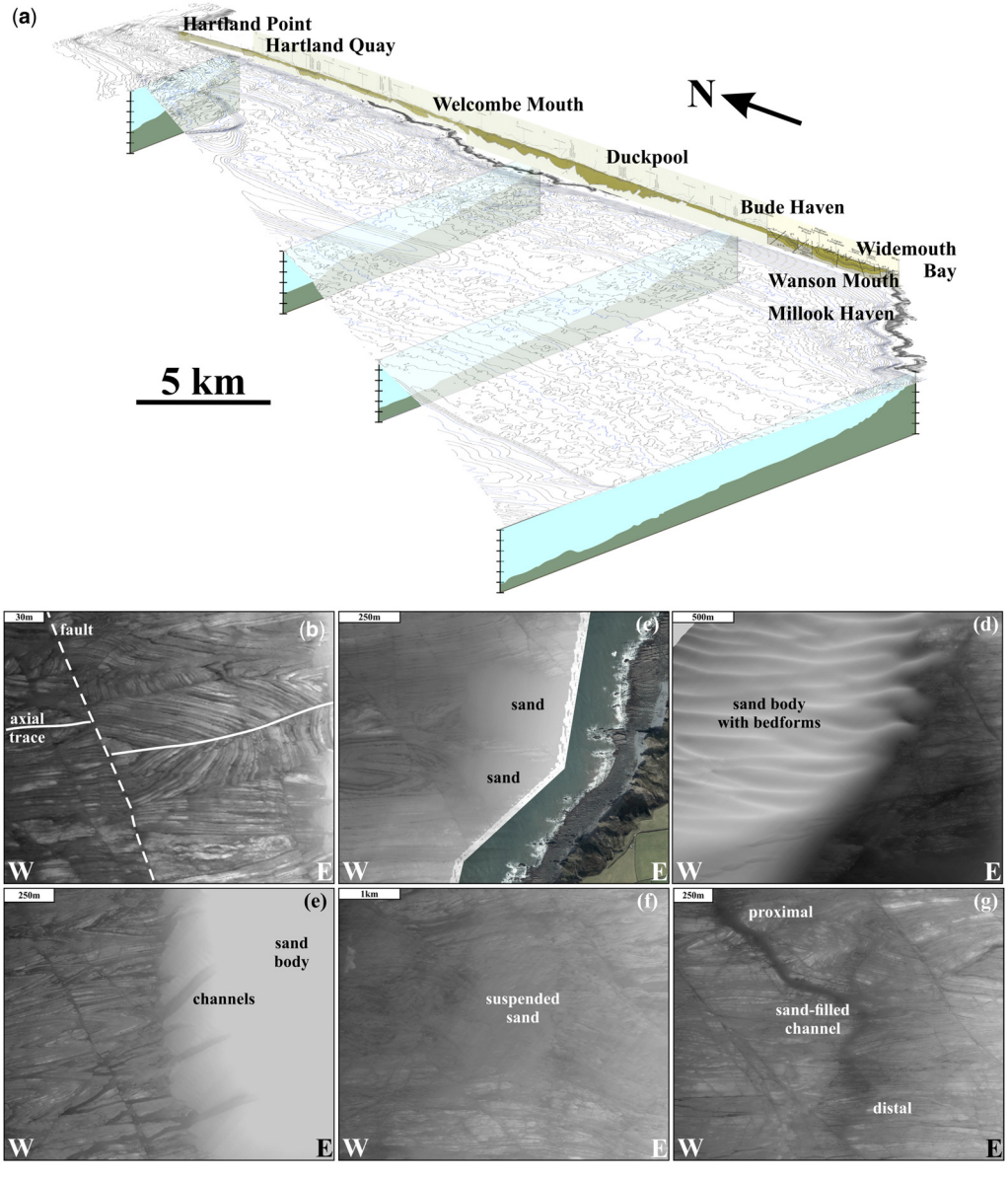

Fig. 5. Seabed topography. (**a**) Contoured bathymetric topological framework of gently sloping seabed, offshore north Cornwall; note, steeper in the north. (**b**)–(**g**) Single-band grey images of: (**b**) exposed seabed showing chevron folds displaced by NNE–SSW faults; (**c**) sand bodies extending from shore; (**d**) offshore sand body with 4 m bedforms; (**e**) offshore sand body with channels; (**f**) suspended sand obscuring seabed; (**g**) suspended sand flowing from north to south and dissipating.

where h is the vertical height of a specific feature (i.e. in the cliff profile). Distortions are progressively >1:1 (i.e. stretched) for plunges <45° and conversely progressively <1:1 (i.e. shortened) for plunges >45°; a plunge of 45° projects undistorted onto a horizontal surface. The chevron folds along the north Cornish coastline are classically defined as upright with plunges of up to *c.* 20° east or west (e.g. Freshney *et al.* 1979). However, much lower plunge angles appear to be more common and therefore have greater impact on the distortion of projections. In general, the effect on upright folds observed

in the cliff profile is an apparent increase in amplitude when projected onto a horizontal plane (i.e. seabed), while wavelength remains effectively constant. Whether features observed in the cliff profile project on to the seabed depends on the plunge azimuth, with only westerly plunging structures observed in the bathymetry.

Vertical to horizontal projection: effect of structural geometry

Structural geometry also affects vertical to horizontal projection and hence subsequent bathymetric map interpretation. Figure 6a shows the subvertical chevron folds at Warren Beach, Hartland Quay, picked out by the Hartland Quay Shale, and the boundary between the Crackington Formation below and the Bude Formation above (Fig. 3). Stereographic analysis indicates that the folds plunge 4° east or landwards, with axial surfaces dipping *c.* 75° south. As such, from equation (1) and assuming cylindrical behaviour, the anticline indicated by the Hartland Quay Shale is projected to close inland *c.* 200 m from the cliff top (Fig. 6b, left). The limbs of this fold are projected to crop out continuously westwards on the seabed, diverging slightly according to their strike. Thus, the seabed outcrop pattern should comprise effectively parallel beds normal to the coastline, repeated by the main anticline and also by any associated minor parasitic folds present (Fig. 6a). To contrast, if we suppose a 4° plunge westwards, the predicted outcrop pattern defined by the Hartland Quay Shale is fundamentally different, again assuming cylindrical behaviour (Fig. 6b, right). The anticline indicated by the Hartland Quay Shale horizon is now projected to close on the seabed *c.* 1500 m offshore and hence its amplitude exhibits significant amplification (stretching) while its wavelength is effectively constant compared with the cliff profile. The parasitic folds on the limbs, again defined by the Hartland Quay Shale, are similarly stretched and amplified, cropping out at relatively large distances (i.e. compared with the height of the cliff) from the shoreline (Fig. 6b, right).

Figure 5c shows the actual bathymetric image of the seabed west of Hartland Quay and adjacent regions. In general, the offshore bathymetry agrees with the 4° E plunge projection (Fig. 6b, left) in that it appears to show an effectively linear structural trend normal to the coastline. However, in detail there are a number of discrepancies, not least because of structures in the seabed that are either not present or are not recognized in the cliff profile and wavecut platform. The most obvious of these is an array of NNW–SSE-trending faults with a dextral displacement sense. The offset of matched fold axes in the wavecut platform suggests that the land outcrops are displaced at least 65 m to the south relative to the seabed outcrops; this offset is matched by the shape of the detailed inset (Fig. 6c), equivalent to the ideal case shown in Figure 6b, left. The expression actually extends approximately twice as far out to sea as the ideal case considers, where it is truncated by a major dextral NNW–SSE fault zone several hundred metres wide.

Vertical to horizontal projection: effect of chevron fold modification

Smaller, subrecumbent chevron folds often occur on the limbs of larger upright chevron folds, with the classic outcrop occurring at Millook Haven (GR 1857 0020; Fig. 1d). However, depending on their plunge, it is not unusual for the recumbent folds to apparently not project onto the adjacent wavecut platform. The configuration of the vertical to horizontal projection and hence the map and/or bathymetric appearance of such recumbent structures therefore may be unexpected. A somewhat simpler example of such 'zig-zag' folds at Welcombe Mouth (GR 2116 1797) illustrates the problems involved.

Whilst the so-called 'Welcombe Diamond' structure (Fig. 7a) appears to be an example of a chevron 'box fold', detailed examination and measurement (see stereonets in Fig. 7b, insets) reveal that the recumbent chevron fold developed after the upright chevron fold: it represents a subsequent modification structure owing to southerly directed subhorizontal shear (Lloyd and Whalley 1997). The aerial view of the wavecut plat form shows a westward/seaward plunging upright synclinal chevron fold, as indicated by the landward converging limbs and dip and younging directions (Fig. 7b); there is *apparently* no indication of the recumbent fold structure owing to the very shallow seaward plunges of both folds. However, the axial trace of the recumbent fold can be projected 43 m northwards to intersect the wavecut platform, where it *appears* to define an upright, tight antiform (Fig. 7b); the fold also crops out in the small water fall along strike in the cliff profile. Figure 7c is a schematic representation of the difference in 3D visualization between the observed (modified chevron fold) structure in cliff profile outcrop and the apparent (upright chevron fold pair) structure in the wavecut platform. In fact, *in-situ* examination in the field reveals that the northern limb of the 'upright antiform' is actually overturned, as indeed it should be.

Thus, initially upright chevron folds subsequently modified by recumbent chevron folds appear geometrically as antiform–synform pairs on the wavecut platform; the characteristic younging

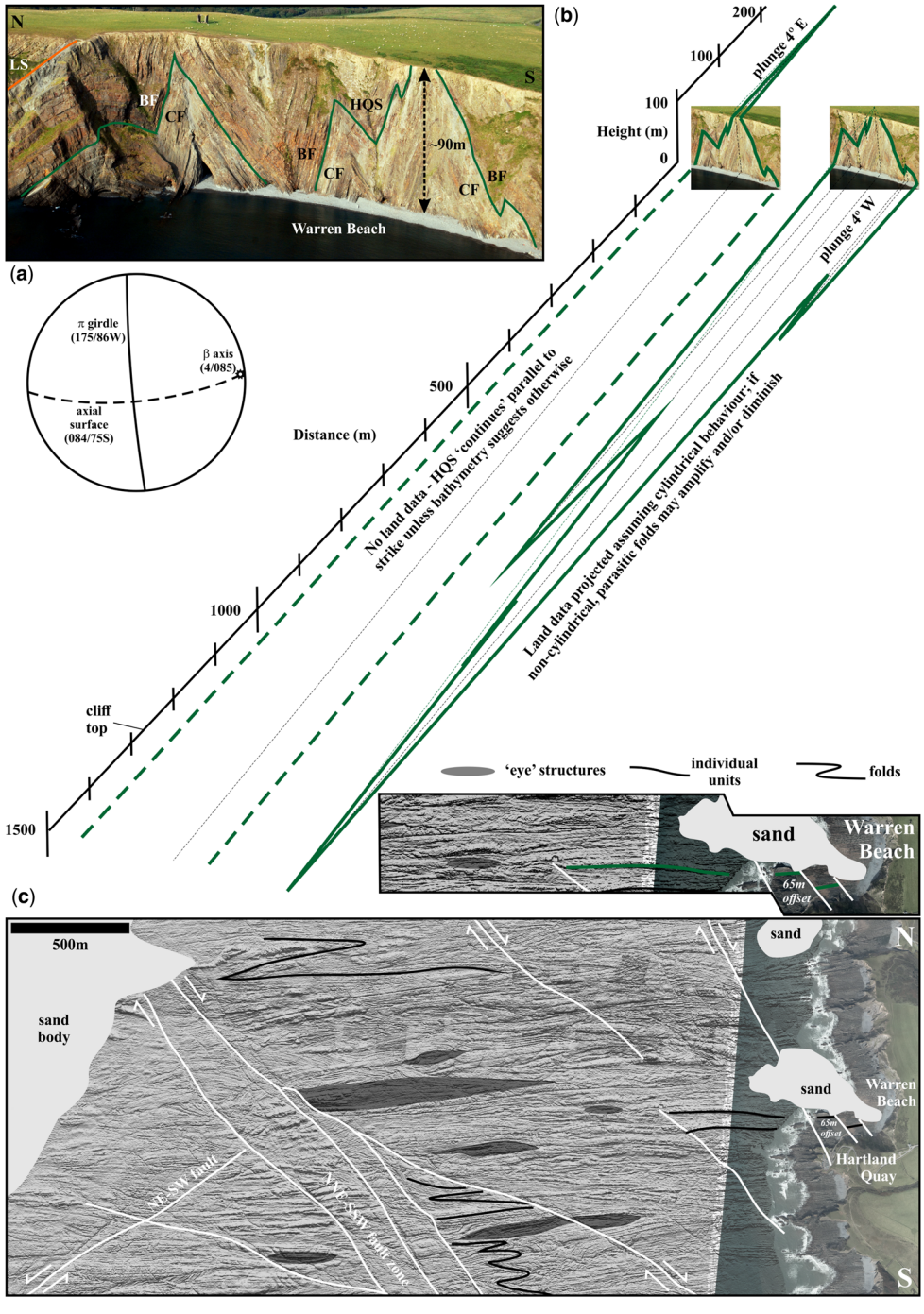

Fig. 6. Vertical to horizontal projection: basic principles. (**a**) Vertical chevron folds, Warren Beach, Hartland Quay, with Hartland Quay Shale (HQS) separating Crackington (CF) and Bude (BF) formations (photograph courtesy of Peter Keene); note stereographic projection. (**b**) Schematic projection of 3D to 2D structural visualization: impact of 4° plunge east (actual) and west on outcrop patterns of upright, cylindrical folds. (**c**) Offshore bathymetry agrees with 4° E plunge projection but is impacted by later faults (white lines) and non-cylindrical periclinal 'eye' structures (shaded); note inset detail box shape, equivalent to (**b**), owing to dextral fault offset.

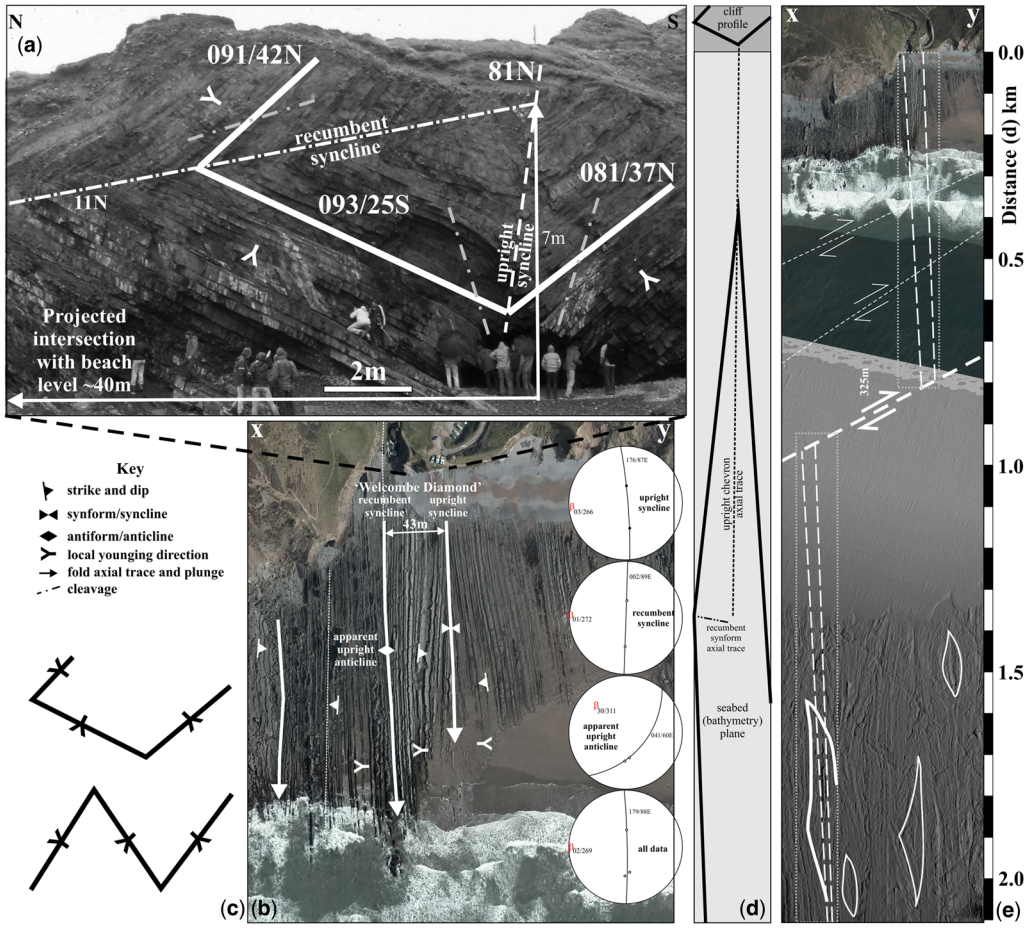

Fig. 7. Vertical to horizontal projection: recumbent folds. (**a**) Cliff profile section of 'Welcome Diamond' structure, Welcombe Mouth. (**b**) Aerial view and interpretation of beach crop of 'Welcombe Diamond' structure. (**c**) Difference in 3D visualization between upright chevron fold pair (below) and recumbent fold modification of an upright synform (above). (**d**) Schematic distinction between upright and recumbent fold vertical to horizontal projections, assuming 3° plunge seawards and scaling defined by the dimensions in the cliff profile. (**e**) Bathymetry offshore Welcombe Mouth; note dextral faults off-setting strike projection and characteristic 'hook' structure, indicative of recumbent chevron folds.

directions can only be recognized *in-situ* in the field. Unfortunately, the wavecut platform appearance is effectively the same as the bathymetric images, which means that it could be potentially difficult to detect and/or distinguish such 'modified' chevron folds in the bathymetry. However, performing a similar analysis to that described in the first example (Fig. 6b) shows that the vertical to horizontal projection of a marker horizon defining the vertical modified chevron fold structure in the cliff profile plane produces a distinctive pattern in the horizontal plane (Fig. 7d). The upright fold axial trace projects seaward parallel to its azimuth (i.e. ~east–west) to intersect the seabed at a distance determined by its plunge (i.e. 3° in this case). In contrast, the projection of the recumbent fold defines an axial trace that trends at a high angle to the east–west, such that the overall projected outcrop pattern has the form of a 'hook' open to the SW.

Such a 'hook' structure is observed in the bathymetry offshore of Welcombe Mouth (Fig. 7e), although its position and geometry may at first appear to be inconsistent with the projection of the Welcombe Diamond structure. The 'hook' structure is offset northwards from the strike of the Welcombe Diamond by *c.* 325 m but this is due to the presence of a NNW–SSE dextral fault (Fig. 5e). It also lies 1.5–2.0 km offshore, which implies a projection

fold plunge of only *c.* 0.3° seaward; the plunge of the Welcombe recumbent fold is 1° seaward at most (Fig. 7b). Finally, the 'hook' structure has a strike length of *c.* 0.5 km, *c.* 50 times the vertical size of the Welcombe Diamond structure (Fig. 7a), but the vertical to horizontal projection distortion is significantly exacerbated as plunge angle deceases towards zero (equation 1 and Fig. 7d).

Vertical to horizontal projection: predicted outcrop geometries

The diverse range of chevron fold geometries observed in the cliff profile along the north Cornish coastline impact critically on the expected seabed outcrop patterns owing to the vertical-to-horizontal projection and plunge/azimuth of fold axial traces. Predicted geometries for an individual marker horizon are shown schematically in Figure 8a to c. Upright chevron folds (e.g. Hartland Quay) project with long, straight limbs relative to the dimensions of the cliff profile (Fig. 8a, left). Even upright parasitic chevron folds can be expected to project similarly (Fig. 8a, right). In contrast, single recumbent modification folds (e.g. Welcombe Mouth) project with elongate, three-sided or 'hook' geometry (Fig. 8b). Ideally, these structures should have axial traces oriented at high angles (i.e. ~north–south) to the typical (i.e. east–west) traces of the upright chevron folds. However, it may be difficult to define a specific axial trace owing to the down-plunge length amplification, which tends to introduce curvature to the limbs (e.g. Fig. 7e). Similarly, multiple recumbent modification folds (e.g. Millook Haven) form 'series' of down-plunge structures, ideally with ~north–south axial traces but practically with curved outlines (Fig. 8c).

Whilst the projections of individual markers shown in Figure 8a to c obviously occur naturally,

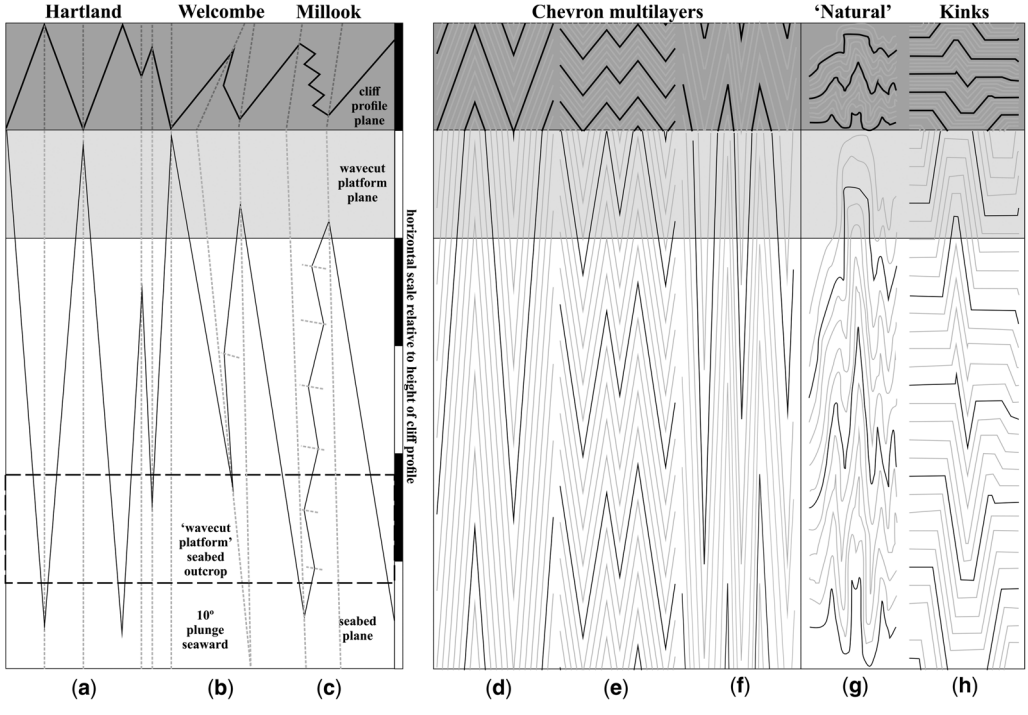

Fig. 8. Schematic summary of predicted seabed outcrop geometries for typical fold structures observed along north Cornish coastline owing to down plunge projection from vertical cliff profile: (**a**)–(**c**) individual marker bed; (**d**)–(**f**) multilayer sequences. Note distinction between the axial traces of original east–west folds and ~north–south modification folds. Scale relative to the width of the wavecut platform. (**a**) Classic upright (left) and parasitic (right) chevrons (e.g. Hartland Quay). (**b**) Single recumbent modification (e.g. Welcombe) resulting in a 'hook-like' structure. (**c**) Multiple recumbent modifications (e.g. Millook) resulting in a down-plunge 'series' structures. (**d**) Chevron folding of multilayers; note layering subparallel to fold axial traces and hinge dilation. (**e**) Multilayer geometry with smaller chevron amplitude. (**f**) Multilayer geometry with variable chevron wavelengths. (**g**) 'Natural' geometry based on experimental model (Fowler and Winsor 1996). (**h**) Kink band folding of multilayers; note layering at high angle to fold axial traces.

they do not do so in isolation; that is, they are projected with many other layers. The Crackington and Bude Formations are multilayer systems typically consisting of relatively thin beds. Figure 8d therefore shows the expected projection of vertical chevron folds developed in such multilayers with the same fold amplitude and wavelength. The vertical-to-horizontal projection amplification results in the development of apparently layered stratigraphic sequences corresponding to each fold limb and hence oriented ~east–west. Note also the dilation in the fold hinge regions, which might promote migration of incompetent units. In contrast, multilayers with smaller wavelength and amplitude chevron folds develop less obvious 'east–west' layering and smaller hinge dilation (Fig. 8e). Figure 8f therefore considers a multilayer sequence with variable chevron fold wavelengths. The resulting seabed outcrop pattern comprises variably oriented stratigraphic sequences, although all trend ~east–west. The spacing of the individual layers also varies with wavelength owing to differences in the limb dips and reflects variations in layer dip on the sea bed. While Figure 8d and e are idealizations, analogue material models of chevron fold development allow an indication of the seabed outcrop patterns that develop naturally (Fig. 8g). In general, natural occurrences are predicted to consist of combinations of the ideal cases. Finally, for comparison, Figure 8h predicts the vertical-to-horizontal projection outcrop pattern expected for folds that develop via kink band formation. The pattern is clearly different from those resulting from chevron folding (e.g. note the occurrence of isolated fold hinge zones and layering at high angles to fold axial traces) and hence provides a means of distinguishing between the two types of folding.

Vertical to horizontal projection: non-cylindrical deformation

The seabed geometries predicted in Figure 8 assume implicitly that the deformation involved was, and hence resulting structures observed in the cliff profile are, cylindrical on the scale of the horizontal distances involved in the seabed projection (i.e. up to several kilometres). However, non-cylindrical fold structures are common along the north Cornish wavecut platform (e.g. Fig. 9a–d), although they are very difficult to recognize in vertical cliff profile sections, and occur with varying plunges, typically towards the east and west. Very similar features are recognized in the bathymetric data (Fig. 9e–h) and are also interpreted to be fold structures owing to non-cylindrical deformation. The presence of non-cylindrical deformation and structures have considerable implications for vertical-to-horizontal projection and the resulting seabed outcrop geometries observed.

Non-cylindrical folds deviate from the ideal cylindrical fold geometry, exhibiting curved hinge lines with changes in trend and plunge. The simplest form of non-cylindrical fold is the pericline or doubly plunging fold, conventionally considered as an antiform (Fig. 10a, left), although synforms also occur (Fig. 10a, right). If the hinge line plunges away from a high point (i.e. the hinge is convex upward), it forms a culmination, whereas if it plunges toward a low point (i.e. the hinge is concave upward), it forms a depression (Fig. 10a, left). However, in practice, many non-cylindrical folds are 'multi-plunging' and form series of antiformal or synformal culminations and depressions (Fig. 10a, right). The occurrence of culminations and depressions on specific combinations of antiform/synform and anticline/syncline can lead to anomalous local geological relationships, such as plunge and younging directions (Fig. 10b). The combination of a parent antiform with a pericline culmination results in 'eye' shapes with older beds in the centre (i.e. antiformal anticlines), while the combination of a parent synform with a pericline depression results in 'eye' shapes with younger beds in the centre (i.e. synformal synclines). In contrast, a parent antiform and pericline depression result in 'eye' shapes with younger beds in the centre (i.e. synformal anticlines), while a parent synform and pericline culmination result in 'closed eye' shapes with older beds in the centre (i.e. antiformal synclines). For the synformal anticline and antiformal syncline cases, the stratigraphical relationships at the 'corners of the eyes' are further complicated and may be reversed (Fig. 10b). Furthermore, the complex outcrop patterns characterized by 'closed eye structures' can occur on different scales within the same overall structure. In some respects therefore, periclinal folds have characteristics similar to refolded folds.

Non-cylindrical fold structures are commonly observed in the bathymetry of offshore north Cornwall, either as single antiformal/synformal periclines culminations/depressions or more complicated 'multi-plunging' structures with multiple axial surfaces (e.g. Fig. 9e–h). For example, many large (i.e. 'mature') chevron folds with long, steep limbs may exhibit periclinal crest lines, resulting in either isolated or a series of eye-fold structures along the axial trace (compare Fig. 9 with Fig. 10c). Alternatively, small periclinal ('immature') folds with short, shallow limbs may develop from individual layers, resulting in 'swarms' of eye-folds within effectively the same stratigraphic level cropping out in complex patterns. Furthermore, hinge lines associated with both 'mature' and 'immature' periclinal chevron folds, but especially the latter, are often limited in length such that they merge

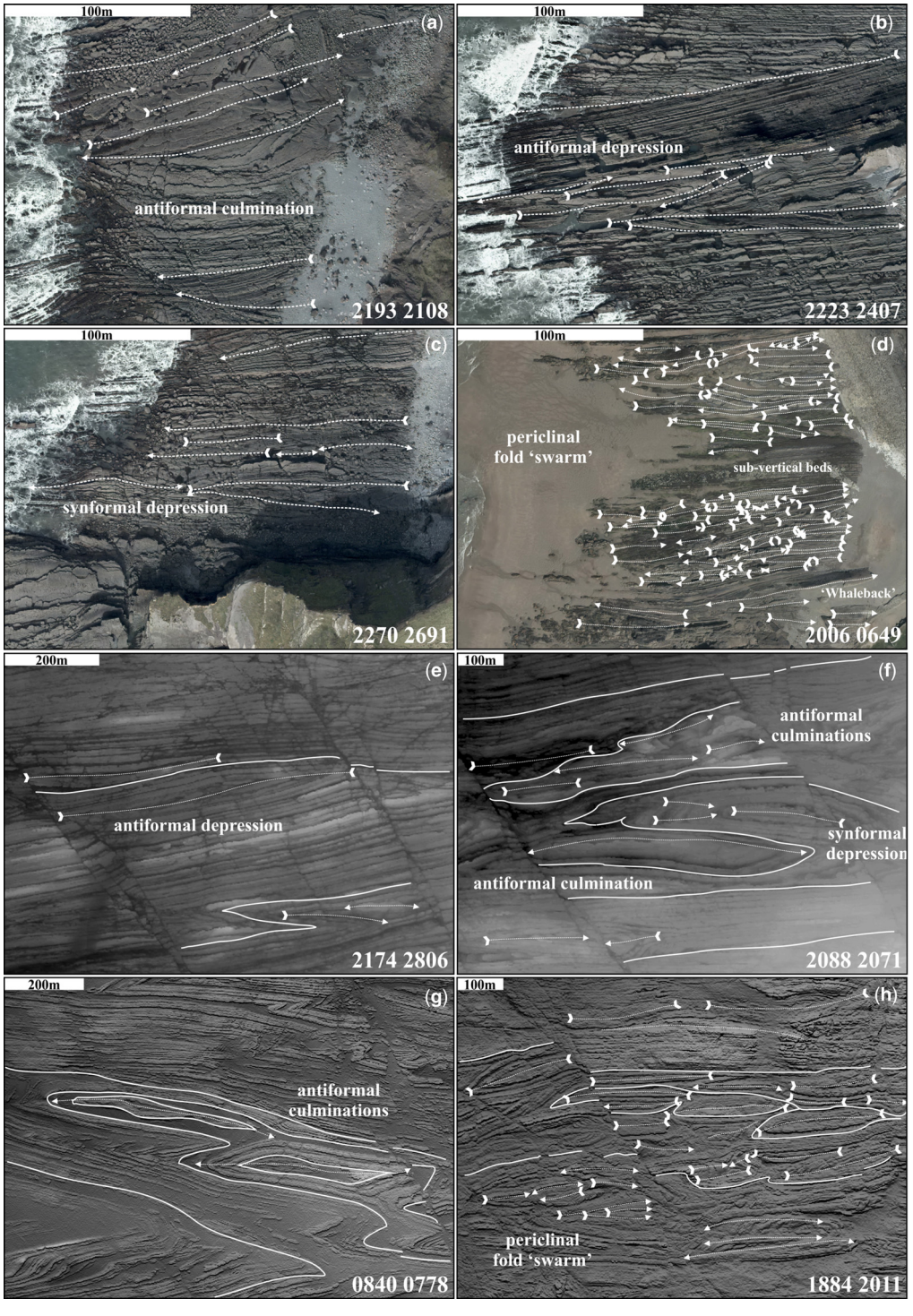

Fig. 9. Examples of individual, double and multiple non-cylindrical (periclinal) fold structures: (**a**)–(**d**) onshore; (**e**)–(**h**) offshore. Broken lines indicate fold axial traces; arrowheads direction of plunge. See Figure 10 for definitions of nomenclature used. Location grid references given lower right.

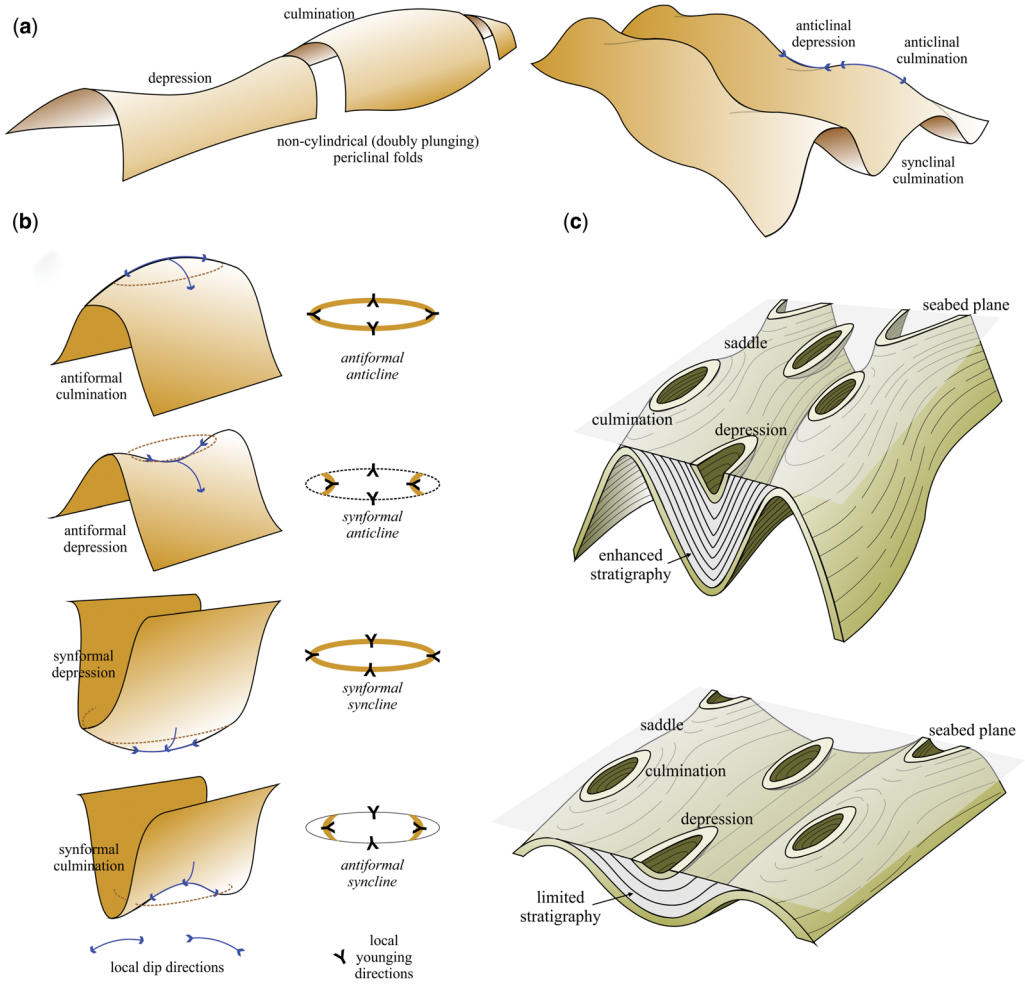

Fig. 10. Non-cylindrical fold geometries. (**a**) *Left*, conventional antiformal pericline with culmination and depression. *Right*, equivalent synformal periclinal forms. (**b**) *Left*, individual upright periclinal forms showing plunge directions of local fold hinge lines. *Right*, predicted outcrop patterns (thick lines) for horizontal sections (thin broken elliptical lines) through periclinal forms. (**c**) *Above*, 'mature' (steep limbed); *below*, 'immature' (shallow limbed) periclinal chevron fold arrays. Source: Figures redrawn from Welker *et al.* (2019) and Ji and Li (2020).

and/or separate in en-echelon patterns linked by 'relay zones' or saddles (Fig. 10c). The result is repetition and apparent expansion of the stratigraphy, usually on a local scale only, which can pose significant problems for interpretation of bathymetry. Natural examples of 'eye-folds' observed in the bathymetry are shown in Figure 9e–f and later in Figures 11a–d and 12.

Structural measurements: QGIS terrain profiles

Interpretation of the potentially complex geological geometries owing to non-cylindrical folding demonstrated in Figures 9 and 10 is facilitated if structural measurements (e.g. strike/dip/sense of bedding, plunge/azimuth of fold axial traces) are available. The bathymetry images of the bedrock offshore north Cornwall and Devon are of excellent quality owing to the relative absence of sediment, either sand bodies on the seabed or dispersed in the sea (e.g. Fig. 5b–g), while there is very little topography on the gently westwards sloping seabed (Fig. 5a). In principal therefore it should be relatively simple to use the Profile tool plugin in QGIS to extract cross-sections and measure the subsea bathymetric data; however, in practice this is not necessarily the case. To illustrate the possible problems, first compare various bathymetric images of a typical

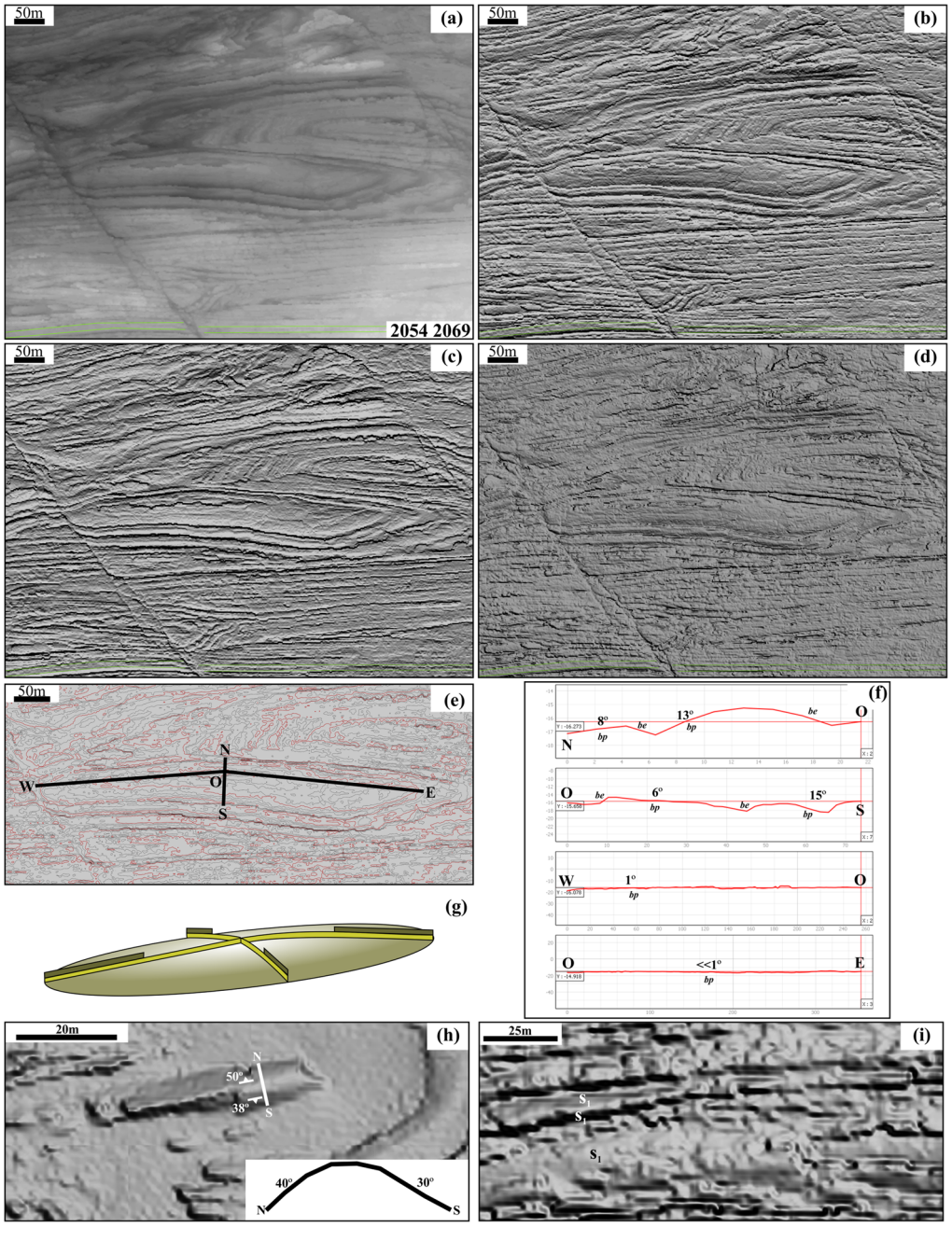

Fig. 11. Structural measurements: terrain profiles, based on periclinal culmination structure. (a–e) Comparison of bathymetric terrain images: (**a**) single-band grey; (**b**) hillshade from north; (**c**) hillshade from south; (**d**) multidirectional hillshade; (**e**) contours (0.5 m minor, 2 m major); note locations of profiles. (**f**) Terrain profiles: N–O–S, 'dip profiles; W–O–E, 'strike profiles; dip angles estimated assuming bedding planes (*bp*) and edges (*be*) correctly identified. (**g**) Schematic representation of periclinal culmination with beds indicated based on profiles. (**h**) LiDAR 'hillshade' (sun from north) image of 'Whaleback' antiformal periclinal culmination, Bude Haven (see Fig. 9d), with field dip and strike of each limb. Also shown, equivalent profile (north–south) and associated dip measurements (inset). (**i**) Bathymetric 'hillshade' (multidirectional) image illustrating problems with identifying bedding planes (potentially $S_{1–3}$).

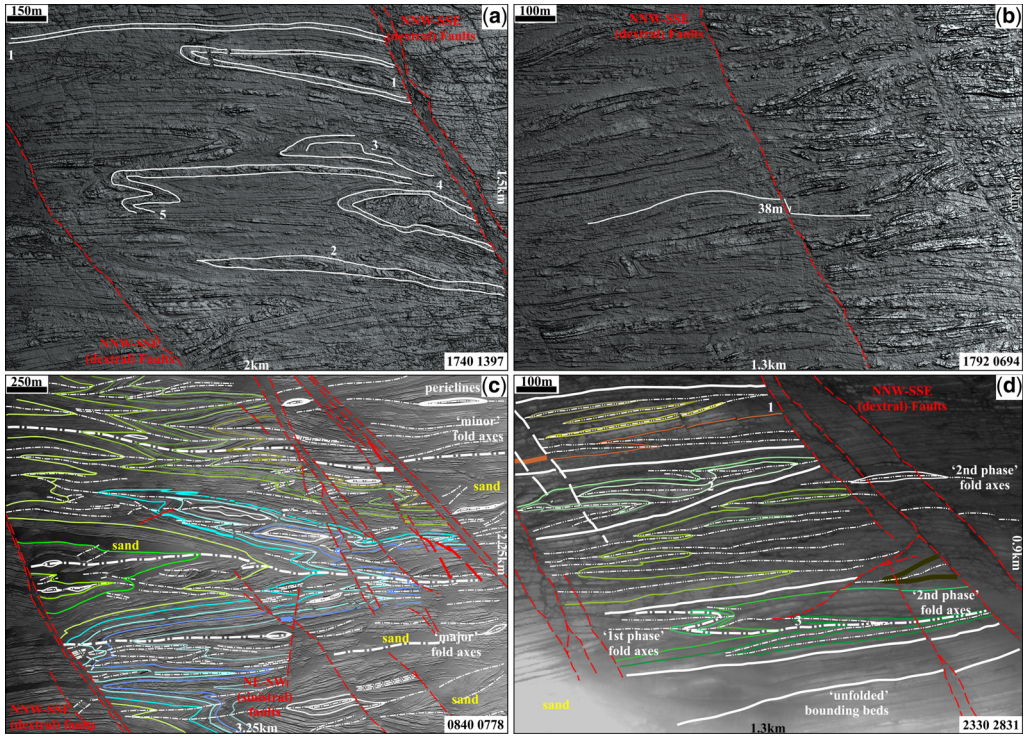

Fig. 12. Examples of colour-coded 'bed' and structure tracing and associated problems; all images combined 'hillshade' (multidirectional) and 'single-band grey rendering. (**a**) Example 1: changes in layer bathymetric characteristics (1, 2) or structural continuity problems (3–5). (**b**) Example 2: problems in matching 'beds' and structures across faults owing to changes in bathymetric characteristics; the possible solution (white traces) indicates a dextral displacement of *c.* 38 m. (**c**) Example 3: extending structural continuity by linking discontinuous stratigraphic units (green and blue lines). (**d**) Example 4: impact of non-cylindrical (periclinal/polyclinal) deformation, note: 1, structural compartmentalization elliptical traces by apparently unfolded 'bounding bed' traces; 2, elliptical ('eye-shaped') 'bed' traces; and 3, apparent 'refolding' – '1st phase' fold axial trace becomes '2nd phase' fold axial trace.

periclinal culmination structure using different rendering schemes. Both 'single-band grey' (Fig. 11a) and 'hillshade sun-north' (Fig. 11b) provide comparable topographic images of the culmination. In contrast, 'hillshade sun-south' (Fig. 11c) suggests that the structure is a periclinal depression. This is known as the Pseudoscopic Illusion (Conklin and Pinther 1976) and it shows that it is very important to determine which is correct if using only 'hillshade' imaging. In our bathymetric mapping, we use combinations of 'hillshade' and 'single-band grey', with the former in 'multidirectional' mode (e.g. Fig. 11d) to attempt to reduce any bias. A further sense-check for whether structures are concave or convex can be performed by determining the highest point of a structure using the simple depth data (Fig. 11a).

The surface of the periclinal culmination is irregular (Fig. 11a, b & d), especially the crest, which could indicate erosion exposing different beds. The irregularity can be quantified in a bathymetric contour image (Fig. 11e) and used to perform terrain profile analyses along specified traverses (Fig. 11f). The potential dips of the pericline culmination limbs and double plunges can then be determined via simple profile trigonometry (equation 1). However, it is uncertain whether the surfaces measured represent bedding planes, as shown schematically in Figure 11g. Indeed, even if the surfaces are bedding planes, it is by no means certain that the terrain profiles provide accurate determinations of dip and plunge. To illustrate this doubt, Figure 11h is a LiDAR image of the 'Whaleback' pericline at Bude Haven (see Fig. 9d). The limb dips measured via terrain profiling are 40° N and 30° S; in contrast, field measurements indicate 50° N and 38° S. The difference is due specifically to terrain profiling effectively averaging dips over a short distance (determined by the spatial resolution of the dataset), whereas field data are measured at discrete points. In

addition, it is often not easy to recognize confidently specific geological surfaces, such as bedding, as illustrated in Figure 10i, where position S_1 represents the curved crest of anticlinal periclinal culmination, S_2 is the edge of a bed and S_3 is a dipping bedding plane. In many situations, it is often difficult to distinguish these positions, especially S_2 and S_3.

Results

Preliminary considerations

The construction of the offshore geological map of north Cornwall essentially involves tracing distinct features in the bathymetry. Ideally, these features represent individual beds (e.g. the 'named' shale horizons in Fig. 3) but in practice may represent bedded units. By tracing the 'beds', the structure (i.e. folds and faults) is hopefully revealed. However, owing to the problems discussed above, this is once again often not as simple as it sounds, as the following simple examples illustrate.

Example 1 (Fig. 12a) shows how the bathymetric appearance of a feature (e.g. individual bed, group of beds or structure) can change significantly along its trace, making continuous tracing difficult. In worst case scenarios, an initially well-defined feature may seem to 'disappear', such that the trace 'jumps' to adjacent, parallel features. Whilst this effect usually maintains the general geometry of the trace, deviations can lead to significant errors in the 'mapping' (e.g. jumping across fold axial traces).

Example 2 (Fig. 12b) illustrates problems that can occur when trying to match 'beds' and/or structures across faults. As for the first example, this is usually due to changes in the bathymetric characteristics of the traced feature across the fault. The worst case scenario is that the feature cannot be matched across the fault and the trace ends. A further complication is that owing to the scale of the mapped area, faults of different lengths are recognized, including their terminations. Thus, assuming the classic elliptical fault model, displacements increase along the fault length from the tips. Further complication is introduced by the coalescence of initially isolated faults, leading to irregular changes in displacement. The net effect is that recognizable displacements on one fault segment may not help to constrain feature matching across another segment.

Example 3 (Fig. 12c) combines the previous examples to show how feature tracing, which is typically limited in length, can be extrapolated over greater distances to extend 'mapping'. This is achieved by recognizing individual traces that overlap at their ends. In the example, two individual but overlapping stratigraphic units indicated by shades of green and blue combine to cover a map area of over 7 km^2. However, the lower right part of the area suffers from bed-tracing recognition problems owing to faults and the partial cover from mobile sediments.

Example 4 (Fig. 12d) illustrates the impact of non-cylindrical deformation on bed tracing (see also Fig. 10). In general, the stratigraphy can be significantly disrupted by the development of periclinal structures. The usual impact is an apparent increase in stratigraphic thickness owing to the same beds being repeated. However, these repeated beds are not necessarily continuous on the seabed owing to the nature of periclinal folding, such that concentric elliptical or 'eye-shaped' 'bed' traces are common. The non-cylindrical deformation therefore tends to 'compartmentalize' individual fold structures and hence 'bed' traces, with 'compartments' bounded by unfolded 'beds' that may or may not connect (eventually) with the periclinally folded 'beds'. In addition, patterns of non-cylindrical (periclinal) fold axial traces often appear to indicate refolding. In the example, an apparent 'first phase' axial trace clearly becomes an apparent 'second phase' axial trace along its length. This contradiction is explained by the nature of non-cylindrical (periclinal) folding, which evolves progressively both spatially and temporally such that different components in the same structure are able to 'overprint' each other. Nevertheless, the results can lead to significant problems for the tracing of individual beds and structures.

Bathymetric geological map, offshore north Cornwall

Our map of the seabed geology, offshore north Cornwall, is shown in Figure 13. Overall, it extends from south to north for *c.* 30 km, from Crackington Haven to Hartland Point, and westwards for *c.* 6 km at Hartland Point progressively extending to a maximum distance of *c.* 20 km in the Bude–Wanson region. These limits are geological: further north into the Bristol Channel, the Lundy Island Tertiary granite intrusion and Bristol Channel Fault Zone interrupt the typical Variscan geology of north Cornwall. To the south, the Carboniferous stratigraphy is increasingly poorly defined. Westwards, the bathymetry is increasingly affected by sand bodies that obscure the seabed geology, while the overall resolution of the bathymetric data reduces as the water depth increases. However, in terms of specific stratigraphy, the mapped area is smaller and covers distances of *c.* 27 km north–south, between Hartland Point and Wanson Mouth, and up to *c.* 10 km east–west, although structures (i.e. folds and faults) can usually be traced over effectively the whole area.

The mapping is based on the composite BGS map cross-sections shown in Figure 4, in particular the named shales in the Crackington and Bude

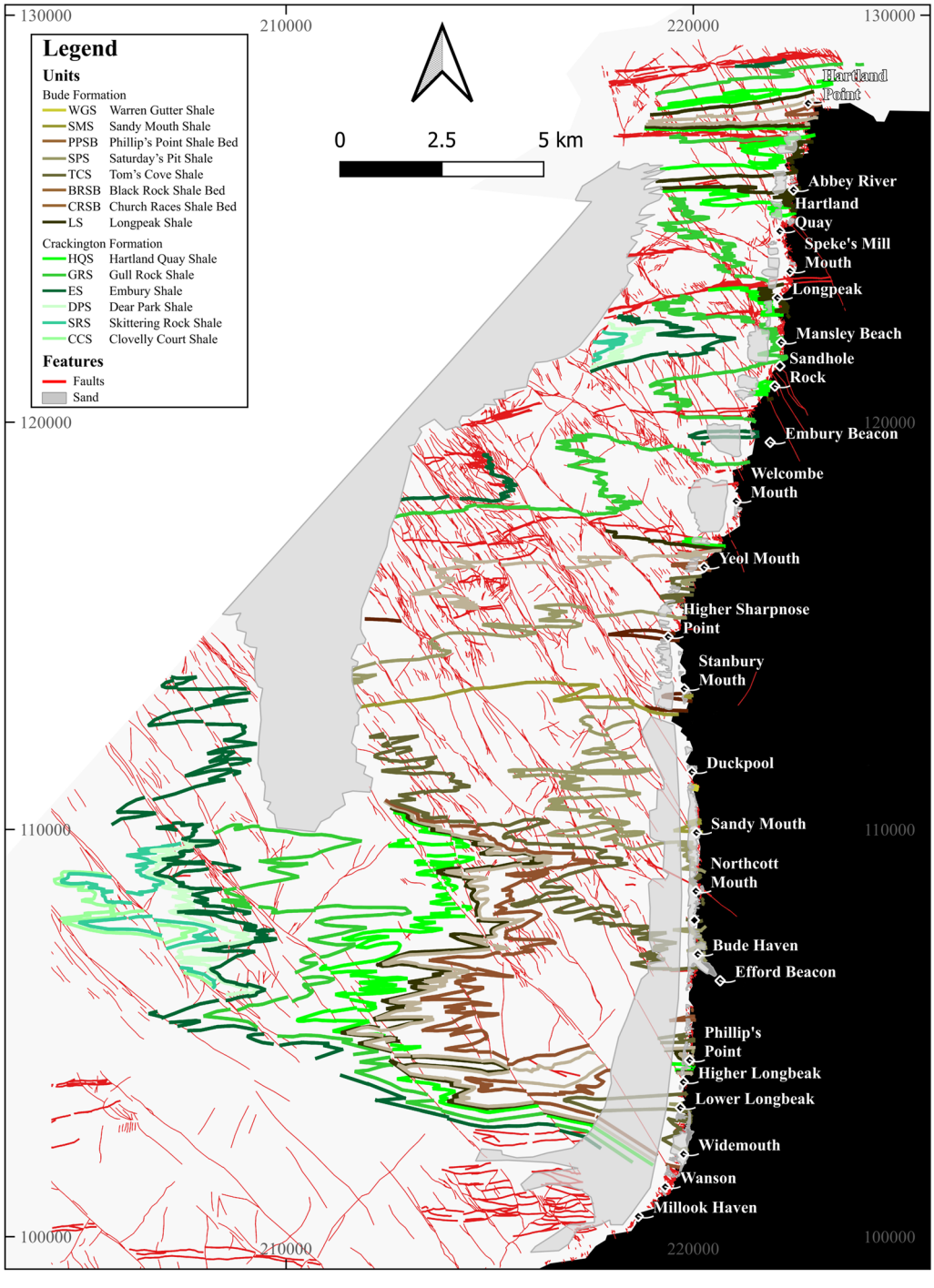

Fig. 13. Bathymetric stratigraphic geological map offshore north Cornwall and Devon – working version. See text for discussion.

Formations shown in Figure 3. The locations of these shales at the base of the cliffs act as marker points from which they project westwards across the wavecut platform and typically out on to the seabed. The wavecut platform outcrops were recognized and traced using high-resolution aerial photographs. However, transition from the aerial photographs to the bathymetry is often interrupted by near-shore sand bodies (i.e. the seaward extension of beaches). In general, there are relatively few locations where the bathymetry and aerial photography intersect continuously (e.g. see Nixon *et al.* 2012) and these usually do not expose the named shales. In addition, numerous faults also traverse the inshore transition region, generally displacing the landward outcrops and hence stratigraphic traces towards the SE relative to the bathymetry. The tracing problems that result, as discussed, are exacerbated by the near-shore sand bodies that cover the faults and hide the displacements.

General description. The stratigraphic map in Figure 13 is colour-coded in terms of the named shales; six (Clovelly Court, Skittering Rock, Dear Park, Embury, Gull Rock and Hartland Quay) in the Crackington Formation and five (Longpeak, Tom's Cove, Saturday's Pit, Sandy Mouth and Warren Gutter) in the Bude Formation (Figs 3 & 4). The boundary between the two formations is defined by the (top of) the Hartland Quay Shale. In addition, several slump bed horizons (Church Races, Black Rock and Phillip's) have also been traced.

The southern half of the bathymetric map between Wanson Mouth and Embury Beacon is dominated by folds on a range of scales. In principal, the main structure is the 'Culm Synclinorium' with its main axis through Duckpool, where the youngest Bude Formation strata (i.e. Warren Gutter Shales) crop out. However, its partner, the 'Culm Anticlinorium', can be recognized immediately to the north through Embury Beacon, where the oldest Crackington Haven units (i.e. Embury Shales) crop out on land, although the wavelength of this structure is perhaps half that of the synclinorium. Nevertheless, both structures are responsible for exposing the whole of the Upper Carboniferous stratigraphy in the bathymetry and adjacent land outcrops.

Further north towards Hartland Quay, folding exposes Crackington Formation stratigraphy both on land and on the sea floor. However, the wavelengths of the folds are noticeably reduced such that the fold limbs appear long and straight, oriented east–west. Fold wavelengths continue to decrease towards Hartland Point, adding to the linear appearance of the outcrop geology.

While the stratigraphic map is restricted to Wanson Mouth to Hartland Point (Fig. 13), south of Wanson Mouth, the Crackington Formation stratigraphy is much less well defined in the BGS cross-sections (Fig. 4) and cannot be used to define location points for bed tracing into the bathymetry. In addition, while the quality of the bathymetry remains good south of Wanson Mouth, the rocks are much fractured, which also makes bed tracing difficult. The increased fracturing is consistent with Late Variscan low-angle faulting of an existing southerly verging overfold and consequent rearrangement of the (Namurian goniatite) stratigraphy (e.g. Freshney *et al.* 1972) and subsequent steep normal and strike-slip faulting (e.g. Peacock 2009).

Faults. At first inspection, perhaps the most obvious features of the bathymetry are faults, as shown in Figure 14. In general, three distinct trends are visible (see also insets in Fig. 14). The first is a dominant NNW–SSE trend comprising mostly dextral strike-slip faults (Fig. 15a, b & f). The second is a less common NE–SW trend comprising sinistral strike-slip faults (Fig. 15a, b), which forms the conjugate set to the first trend. Both of these trends populate the whole map area and have been studied previously both on land and via bathymetry by Nixon *et al.* (2012). In contrast, the third trend occurs in more restricted locations, specifically south of Wanson Mouth and also north of Marsland Mouth, and comprises east–west-oriented faults (Fig. 15d, e). Whilst displacement senses on the strike-slip faults are generally easy to recognize, this does not apply to the east–west faults, not least because they are typically parallel to the regional strike of bedding. However, they are displaced by and hence pre-date the conjugate strike-slip faults. Based on published work in this area (Enfield *et al.* 1985; Selwood *et al.* 1985; Selwood and Thomas 1985, 1986; Whalley and Lloyd 1986; Warr 1989; Le Gall 1990, 1991; Mapeo and Andrews 1991; Thompson and Cosgrove 1996; Lloyd and Chinnery 2002) they are considered to be (bedding parallel) Variscan thrust structures with both North (fore) and South (back) propagation senses.

The NNW–SSE fault array is clearly the most common and also consists of the longest faults (Fig. 15a). The NE–SW conjugate array appears to act almost like rungs in a ladder connecting adjacent NNW–SSE faults (Fig. 15b). It is possible therefore that the slip on the NNW–SSE set induces subsequent slip on the other set, which would be compatible with the behaviour of a Reidel-type system. Nevertheless, both sets post-date the thrusting and folding, which they clearly displace (Fig. 15d, f–i). However, not all apparently NNW–SSE or NE–SW faults are necessarily part of this conjugate system. Some faults are restricted in range and occur in 'domino-style' arrays (e.g. Fig. 15c). These faults appear to be related to flexural slip deformation between layers, presumably during chevron folding.

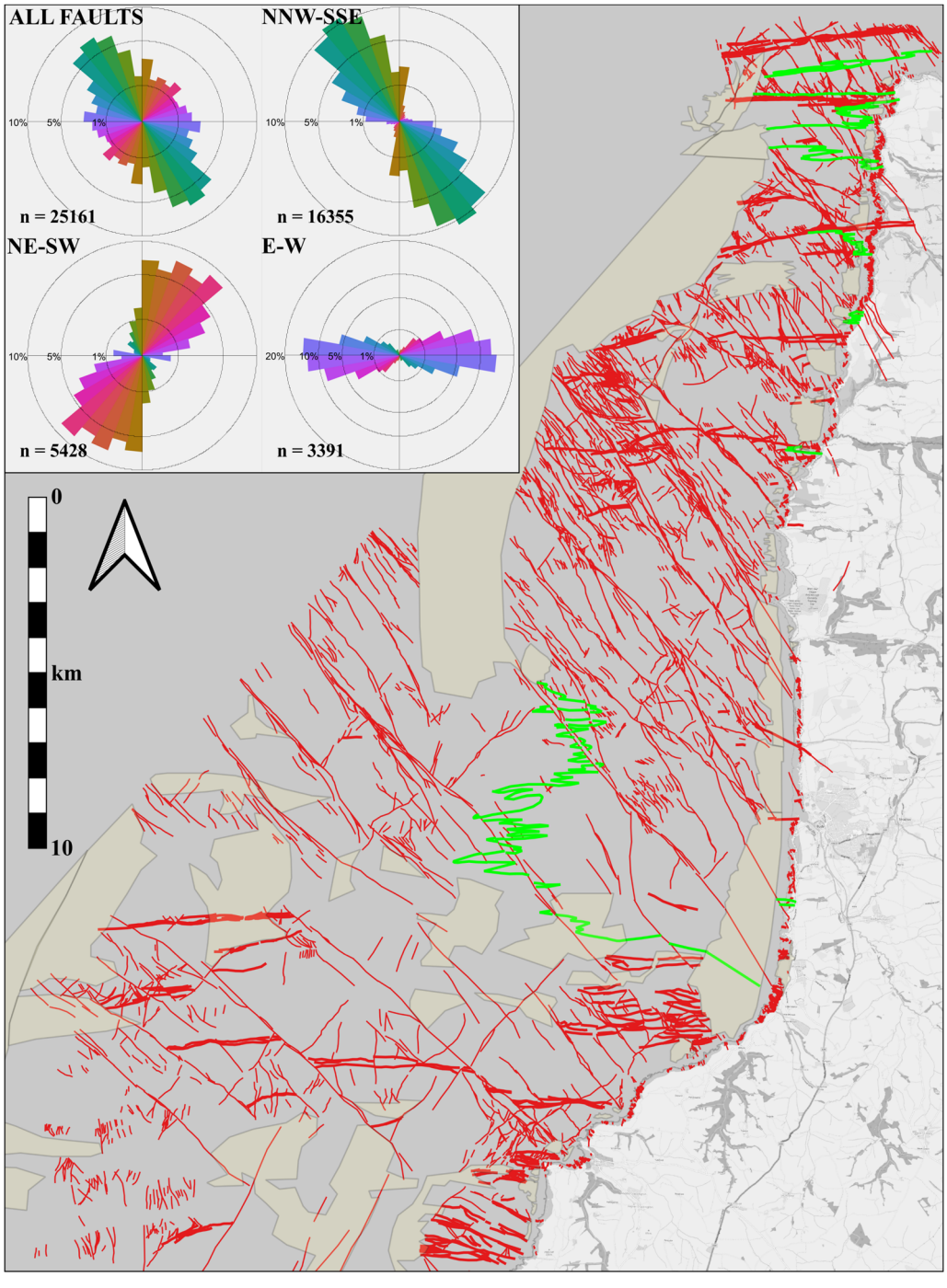

Fig. 14. Fault map of offshore north Cornwall, showing three dominant arrays: 1, dextral NNW–SSE; 2, sinistral NE–SW conjugate strike-slip faults; and 3, east–west thrusts, either north (fore) or south (back) propagating. Also shown is the boundary (green, Hartland Quay Shale) between Crackington and Bude formations and main sand bodies. Inset: rose diagrams of all, NNW–SSE, NE–SW and east–west fault segments create using FracPaq (Healy *et al.* 2017).

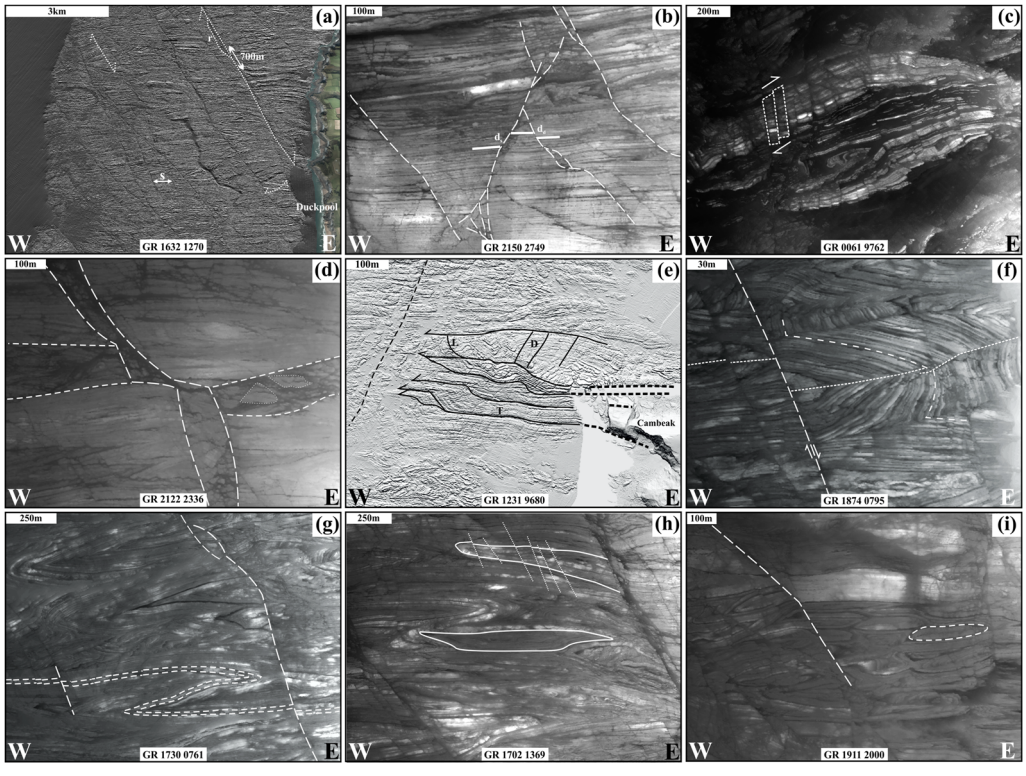

Fig. 15. Examples of bathymetric images (*single-band grey* unless stated) of fault structures, offshore north Cornwall. (**a**) NNW–SSE trending regional and smaller scales (strike-slip) faults with dextral displacements, relay zones (r) and splays (s); note also linking NE–SW sinistral faults. *Hillshade*, 'sun' from north. (**b**) NE–SW faults with sinistral displacements linking larger scale NNW–SSE faults. (**c**) Domino-style fault array possibly due to bed-parallel shear. (**d**) Dextral displacement of broad east–west, approximately bedding-parallel, thrust fault zone by NNW–SSE fault. (**e**) Westerly propagating (lateral) bedding-parallel thrusts; note domino and listric faults. *Hillshade*, 'sun' from N LiDAR image of coast lower right). (**f**) Chevron folds displaced dextrally by NNW–SSE faults. (**g**) 'Stack' of kilometre-scale ('isoclinal') chevron folds displaced by NNW–SSE faults of different scales. (**h**) Faulted 'eye' section through periclinal fold. (**i**) Multiple NNW–SSE faulted periclinal folds.

They must therefore be syn-folding in age and predate the conjugate faults.

The dominant NNW–SSE dextral strike-slip faults are almost certainly part of the same system recognized on land and in particular the Sticklepath–Lustleigh fault zone, which traverses the whole SW England Peninsula and extends in to both the Bristol and English Channels (e.g. Dearman 1963). The dextral displacement has been dated as Late Variscan, which offsets earlier Variscan thrusts (Holloway and Chadwick 1986), compatible with observations in the bathymetry map (Figs 13–15). However, Holloway and Chadwick (1986) also recognized evidence for early Tertiary (probably Oligocene) sinistral movement on the Sticklepath–Lustleigh fault zone, forming pull-apart basins, followed by minor dextral movement in the mid-Tertiary. The significance of these observations is for fault reactivation from Variscan to almost Present times. Kim *et al.* (2001) have also recognized reactivated strike-slip faults onshore at Crackington Haven. Evidence for similar reactivation in the faults mapped via bathymetry is more difficult to ascertain as only the final (cumulative) displacement is observed but some NNW–SSE faults exhibit finite sinistral displacement and conversely some NE–SW faults exhibit finite dextral displacement. Evidence for reactivation of the east–west faults, whether by normal, reverse or strike-slip movement, is absent. Nevertheless, in general, any fault is capable of reactivation in a subsequent appropriately oriented stress field, as Peacock (2009) discusses.

Folds

The offshore region of north Cornwall contains hundreds of folds on a wide range of scales, as shown Figure 16a. These are dominated by the east–west

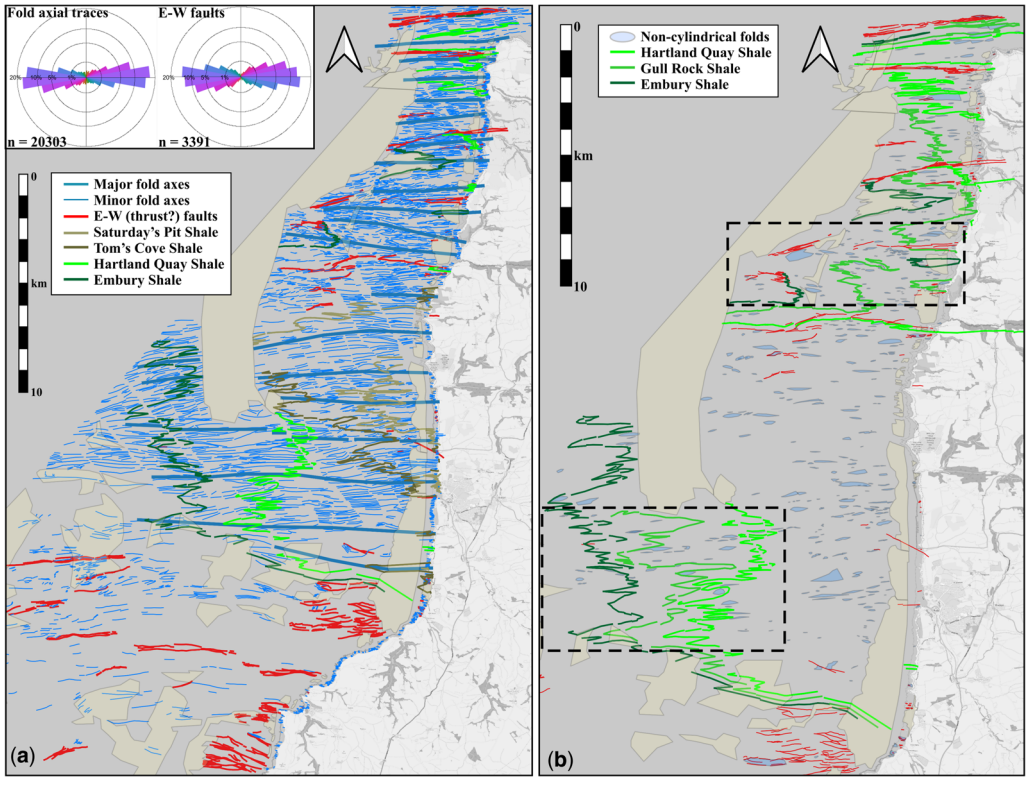

Fig. 16. Summary maps of offshore fold structures. (**a**) Major (thick blue) and minor (thin blue) fold axial traces (blue); two thickest lines indicate axes of Culm Synclinorium and Anticlinorium through Duckpool and Elmscott respectively. Also shown, boundary (green, Hartland Quay Shale) between Crackington and Bude Formations, east–west (thrust) faults (red) and main sand bodies. Inset, rose diagrams of fold axial trace and fault orientations created using FracPaq (Healy *et al.* 2017). (**b**) Non-cylindrical (periclinal) fold structures (blue) distribution. Also shown, Upper Crackington Formation shales indicating regions of 'expanded' stratigraphy (boxes), east–west (thrust) faults (red) and main sand bodies.

essentially upright chevron folds but also include the essentially recumbent chevron modification folds, which share the same general axial trace orientation (e.g. see Fig. 6a for an example of both styles). Most of the folds are apparently easterly plunging, although westerly plunging structures do occur as well, often contributing to doubly plunging periclinal folds (see below). Most of these folds form part of a number of major regional scale fold structures on the scale of *c.* 1–5 km (Fig. 16a). In addition, these regional folds also combine to form not only the well-known 'Culm Synclinorium', which has its axial trace approximately through Duckpool, but also an equivalent 'Culm Anticlinorium' further north with its axial trace through Elmscott (GR 2230 2310). It is interesting to note that both the fold axial traces and trends of the east–west (thrust) faults are effectively identical (Fig. 16, inset), which suggests that these structures either formed contemporaneously and/or under similar stress systems (i.e. maximum, intermediate and minimum principal stresses oriented either subhorizontally ~north–south, ~east–west and/or subvertical respectively).

Many of the folds recognized in the bathymetry are part of either doubly or multiple plunging periclinal structures (e.g. Figs 9, 11 & 15) and formed owing to non-cylindrical deformation. Figure 15b shows the distribution of non-cylindrical fold structures recognized in the bathymetry, although it is emphasized that more are present on scales ranging from tens to hundreds and indeed potentially thousands of metres. The structures are typically elongate/elliptical ('eye-shaped') and oriented east–west, parallel to the trend of the fold axial traces in general. It seems therefore that the chevron folding deformation, and therefore probably the thrust faulting, in this region was non-cylindrical in general. The distribution of the non-cylindrical folds has a significant impact on the stratigraphic outcrop pattern, depending on whether the folds and fold

limbs are steeply (i.e. form 'mature' chevron) or shallowly (i.e. form 'immature' chevrons) dipping and plunging (see Fig. 8c). The former results in rapid changes in stratigraphy, whereas the latter results in restricted stratigraphy over significant area. Thus, areas of 'mature' periclinal chevron folds are associated with almost true bed thicknesses in outcrop and hence normal stratigraphic separations (i.e. between the 'named' shales), often associated with long, straight east–west limbs extending for up to several kilometres (e.g. from Wanson Mouth, Gr 1950 0150, Litter Mouth, GR 2070 1700, and Hartland Point, GR 229 276). In contrast, areas of 'immature' periclinal chevron folds are associated with exaggerated apparent bed thicknesses in outcrop and hence apparently increased stratigraphic separations. The latter behaviour is especially noticeable in the core of the 'Culm Anticlinorium' and also offshore north and south of Bude, where it is responsible for exposing almost all of the Bude Formation (Fig. 16b).

Discussion

Despite the undoubted spectacular bathymetry data available for offshore north Cornwall, as well as the apparently well-known coastal geology, it is nevertheless far from a simple matter to extrapolate from land to the sea. An honest appraisal is that the bathymetric geological maps produced in this contribution, particularly of the stratigraphy, are unlikely to be truly accurate representations although significantly better and more reliable than extrapolating structure found in outcrops further offshore. The main reason for this assessment concerns the veracity of the stratigraphic framework (Fig. 3) and the structural cross-section interpretation (Fig. 4), on which the bathymetric mapping is ultimately based. In particular, although the precise fossil localities given by the BGS for 'named shales' represent tight constraints, they are limited and diminish from each locality.

Consider the available fossil markers: while most stratigraphic correlations in the British Upper Carboniferous are based on bio-stratigraphic criteria, two types of 'marker horizon' are also available. The most widely used are marine bands, particularly in the upper Namurian to middle Westphalian (Yeadonian to Bolsovian), which include the Crackington and Bude Formations (e.g. Calver 1968, 1969; Ramsbottom 1969, 1971, 1977, 1978, 1979). Alternatively, cineritic tonsteins owing to volcanic ashfalls have proved useful where marine bands do not occur (e.g. Bouroz 1967), although they have not been widely used in Britain (e.g. Burger 1985; Leeder 1988). North Cornwall includes the upper part of the Crackington Formation between the Embury, Gull Rock and Harland Quay Shales. All three shales contain diagnostic fossils (i.e. G. subcrenatum, G. listeri and G. amaliae respectively). Elsewhere in SW England, older Crackington Haven beds occur, with fossiliferous shales (e.g. Clovelly Court, Skittering Rock and Dear Park) recognized in the Upper Namurain (Yeadonian) that also contain diagnostic fauna (Fig. 3). Thus, the exposed Crackington Formation extends from the base of the Langstettian (Westphalian A), represented by the Embury Shale, to its top, defined by the Hartland Quay Shale, and appears to be well constrained stratigraphically (Fig. 3).

Unfortunately, the same level of biostratigraphical constraint is not possible for the Bude Formation, which makes up most of the geological outcrop, both on land and subsea. Although the Bude Formation is at least 1290 m thick, marker beds are generally restricted to five black sulfurous mudstones (King 1967; Freshney and Taylor 1972): Longpeak, Tom's Cove, Saturday's Pit, Sandy Mouth and Warren Gutter shales (Fig. 3). However, the fossils in the lowest three shales are of little biostratigraphical use, although the Tom's Cove Shale might be correlated with the Vanderbeckei Marine Band of South Wales (Edmonds in Ramsbottom *et al.* 1978). Thus, only the youngest two Bude Formation marine bands, which effectively bracket the upper half of the formation, therefore appear to contain diagnostic fauna. The Sandy Mouth Shale contains the holotype of *Anthracoceratoides cornubiensis* Ramsbottom (Ramsbottom 1970), one of the most characteristic ammonoids of the Langsettian Culm that probably indicates a correlation with the Meadow Farm Marine Band in South Wales. The Warren Gutter Shale has yielded a diverse assemblage including the ammonoid *Donetzoceras aegiranum* Schmidt (Freshney *et al.* 1979), previously referred to as *Anthracoceras aegiranum* Schmidt (Saunders *et al.* 1979), a distinctive index taxon indicative of the Aegiranum Marine Band (Cleal and Thomas 2013). Thus, the fossil constraint on the biostratigraphy of the Bude Formation is clearly limited at best.

Assuming that the onshore stratigraphy is well constrained, bathymetry-based mapping of offshore north Cornwall (Fig. 13) should be reliable as long as appropriate features identified onshore as the specific shale marker horizons can be followed offshore. As discussed previously, this often cannot be achieved with confidence for a number of reasons. In the first instance, near-shore sand bodies (e.g. extensions of beaches), which often cover strike-slip faults as they run onshore, typically obscure the contact between land and seabed outcrops for up to a kilometre seawards, making it difficult to link a stratigraphic reference bed recognized onshore to the bathymetry, even taking in to account vertical to horizontal projection. Furthermore, where a link

between onshore and offshore features can be achieved, rapid variations in bathymetric image characteristics often make bed tracing in the bathymetry difficult (Fig. 12a). However, the essential geometry of the trace can usually be maintained, and indeed extended by linking overlapping discontinuous stratigraphic units (Fig. 12c), except in two unfortunately common situations. Firstly, where the trace crosses a fault, especially one with large displacement, it may then be difficult to determine the offset of the trace (Fig. 12b). The second situation is due to the geometry of chevron folding, which can be either cylindrical or non-cylindrical. For cylindrical folds (Figs 8 & 12b), fold amplitude can vary rapidly: anticlinal/synclinal closures can divide and grow in to multiple anticlines/synclines, and it is even possible for anticlines and synclines to apparently 'confront' each other. For non-cylindrical folds (e.g. Figs 10c & 12d), 'mature' periclinal chevron folds, especially where occurring in 'swarms', can compartmentalize regions between apparently unfolded long, straight 'bounding' beds; in between, 'immature' periclinal chevron folding can result in complex patterns of repeated and restricted stratigraphy that easily obfuscate bed tracing. It may also be difficult to simply trace the detailed structure within the bathymetric images.

Owing to the effectively continuous strike-normal outcrop offered by the cliff profile and wave-cut platform along the north Cornwall and Devon coastline, it is generally considered that the structure is well constrained (e.g. Fig. 4). Unfortunately, this is not the case, which is where bathymetric data can help. The structural model is effectively based on the detailed mapping by King (1967) (see also Freshney *et al.* 1972, 1979; Freshney and Taylor 1972) between Wanson Mouth and Bude Haven, which in turn is based on his stratigraphy constrained by the Tom's Cove Shale as a datum (Table 1). As such, the stratigraphy is effectively based on lithological characteristics that are followed through the outcrop to constrain the structure. However, although the section constructed appears rigorous, there are several problems. The sequence represents the lowest part of the Bude Formation, which is devoid of biostratigraphical markers (*Rhabdoderma elegans* is not considered diagnostic). Sandstones in the Bude Formation, even the thickest, are laterally impersistent with thicknesses varying. The lowest *c.* 300 m and top of the sequence are based on slump beds, which are difficult to correlate.

For example, King (1971) names two slump beds (Lynstone and Black Rock) at 130–150 m beneath the Tom's Cove Shale (Table 1), which he correlates as being equivalent in different parts of his section (e.g. Fig. 4). Unfortunately, the sequence is not continuously exposed south of Tom's Cove to the Black Rock exposure, while northwards a major fault zone in the section is recognized at Phillip's Point. Whilst the BGS map cross-section states that the nature of the fault zone (i.e. fault type, offset, sense of displacement) is unknown, the assumption in the stratigraphic and structural sequences is that it is a normal fault which is down-thrown to the north. To restore horizons across the fault requires *c.* 500 m displacement, which would imply a regional scale fault in the area for which there is no evidence inland. An alternative explanation is that the fault was originally a northerly propagating thrust that has been subsequently rotated into a normal fault configuration by chevron folding modified by southerly directed shear (e.g. Sanderson 1979; Lloyd and Whalley 1997). Support for this interpretation is provided by Enfield *et al.* (1985) from a demonstrably chevron folded and southerly overturned initially northerly propagating thrust structure just north of the main fault zone. Similar explanations for large-scale thrusts subsequently rotated to appear as normal faults have been suggested for the Wanson North Fault, the tectonic boundary between the Bude and

Table 1. *Stratigraphic position and characteristics of members in the Bude Formation, using the base of Tom's Cove Shale as a datum (after King 1971)*

Stratigraphic position (metres)	Member	Characteristics
230–240	Phillip's	'Slump bed'
115–125	Saturday's Pit	Black shale with nodules
70–105	Upton Cross	Major sandstone unit
0–20	Tom's Cove	Black shale with nodules containing coelacanthid *Rhabdoderma elegans*
30–50	Earthquake	Major sandstone unit
70–90	Efford	Shale with siltstone above containing xiphosurid trails
130–150	Lynstone	'Slump bed'
130–150?	Black Rock	'Slump bed'
270–280	Church Races	'Slump bed'

Crackington formations (Enfield *et al.* 1985) and the Rusey Fault Zone (Warr 1989; Thompson and Cosgrove 1996). On the intra-formational scale, Lloyd and Chinnery (2002) have suggested that the whole of the Bude Formation can be considered as a three-dimensional, Variscan imbricate stack comprising and stratigraphically thickened by both northerly and southerly propagating fore and back thrusts, none of which are currently recognized in the structural cross-section for north Cornwall (Fig. 4); major thrust structures interpreted from seismic surveys (Le Gall 1990, 1991) are also missing.

In summary, the historical stratigraphic and hence structural frameworks of both the Crackington and especially Bude Formations of north Cornwall are of questionable validity. Such unreliability must propagate therefore into the geological interpretation of the bathymetry and hence the geological map presented here for offshore north Cornwall. Much further work is clearly necessary, both on land and subsea, in order to reconcile the onshore and offshore geology.

Conclusions

Bathymetric images of offshore north Cornwall and Devon are undoubtedly spectacular and it would appear therefore to be a relatively simple matter to construct viable geological maps of the seabed by simply extrapolating the known onshore geology (e.g. based on BGS cross-sections). Unfortunately, the reality is not that simple and even the maps produced in this contribution are unlikely to be accurate for a number of reasons. These include: (1) the veracity of the stratigraphic basis for the geology of the coastline; (2) the significance of vertical to horizontal projection; (3) the presence of regional-scale non-cylindrical deformation; (4) potential measurement problems (e.g. dips) using terrain profiles, resulting in a complete absence of dip and fold plunge data in the final map; and (5) variations in bathymetric image characteristics which make feature tracing difficult, although these can be mitigated by imaging techniques that have not been attempted here, compounded by displacements across faults and adverse impacts of sand bodies and sediment dispersions. Each of these factors introduces potential problems for bathymetric interpretation and they collectively make the construction geological maps of offshore north Cornwall and Devon far from a simple matter. Nevertheless, the maps constructed do represent a valid basis for subsequent improved understanding of this region by continued, careful and detailed mapping.

Acknowledgements This contribution contains UK Hydrographic Office data © Crown copyright and database (https://data.admiralty.co.uk/portal/apps/sites/#/marine-data-portal). We thank the UK Hydrographic Office for providing the multibeam bathymetry data HI 1158 (Barnstaple Bay Part 2) and HI 1157 (Hartland Point to Land's End Blk1) under Bathymetry Data License v.1. Aerial photography was provided by the Channel Coastal Observatory (www.channelcoast.org). Thanks also to Peter Keene for his aerial photograph used in Figure 6.

Competing interests The authors declare that they have no known competing financial interests or personal relationships that could have appeared to influence the work reported in this paper.

Author contributions **BC**: data curation (equal), methodology (equal), resources (equal), software (lead), visualization (equal), writing – review & editing (equal); **GEL**: conceptualization (lead), data curation (equal), investigation (lead), methodology (equal), project administration (equal), resources (equal), visualization (equal), writing – original draft (lead), writing – review & editing (equal).

Funding This research received no specific grant from any funding agency in the public, commercial, or not-for-profit sectors.

Data availability The datasets generated during and/or analysed during the current study are available in the Channel Coast Observatory repository, and the Admiralty Data Portal, https://coastalmonitoring.org/, https://datahub.admiralty.co.uk/.

References

Bouroz, A. 1967. Correlations des tonsteins d'origine volcanique entre les bassins houillers de Sarre-Lorraine et du Nord-Pas-de-Calais. *Compte Rendu Hebdomadaire des Seances de l 'Academie des Sciences Serie D Science Naturelle, Paris*, **264**, 2729–2732.

Burger, K. 1985. Kohlentonsteine in Kohlenrevieren der Erde. *Erkenntnisstand 1983. Compte Rendu 10 me Congress Internationale Stratigraphie Geologique Carbonifere*, 1983, Madrid. **I**, 155–174.

Burgmann, R., Rosen, P.A. and Fielding, E.J. 2000. Synthetic aperture radar interferometry to measure Earth's surface topography and its deformation. *Annual Review of Earth and Planetary Sciences*, **28**, 169–209, https://doi.org/10.1146/annurev.earth.28.1.16

Calver, M.A. 1968. Distribution of Westphalian marine faunas in northern England and adjoining areas. *Proceedings of the Yorkshire Geological Society*, **37**, 1–72, https://doi.org/10.1144/pygs.37.1.1

Calver, M.A. 1969. Westphalian of Britain. *Compte Rendu du 6ème Congrès International de Stratigraphie et de Géologie du Carbonifère*, 1967, Sheffield, 233–254.

Claoue-Long, J.C., Roberts, J. and Jones, P.J. 1993. Carboniferous time. *Early Carboniferous Stratigraphy (Abstracts), IUGS, Sub-Commission on Carboniferous Stratigraphy*, Liege, Belgium.

Cleal, C.J. and Thomas, B.A. 1996. *The Culm Trough. British Upper Carboniferous Stratigraphy*. Geological Conservation Review Series No. 11, JNCC, Peterborough.

Cleal, C.J. and Thomas, B.A. 2013. The Culm Trough. *In*: *British Upper Carboniferous Stratigraphy*. Geological Conservation Review, **11**. Chapman and Hall.

Conklin, H.C. and Pinther, M. 1976. Pseudoscopic Illusion. *Science (New York)*, **194**, 374, https://doi.org/10.1126/science.194.4263.374.a

Cracknell, A.P. and Hayes, L. 2007. *Introduction to Remote Sensing*. Taylor and Francis, London.

Davison, I., Jeffcoate, A. and Oing, H. 2004. Geometry of chevron folding shortening and estimates at Hartland Quay, North Cornwall, UK, and some regional implications for Culm Basin development. *Proceedings of the Ussher Society, Geoscience in South-West England*, **11**, 42–50, http://ussher.org.uk/wp-content/uploads/journal/2004/07-Davison_et_al_2004.pdf

Dearman, W.R. 1963. Wrench-faulting in Cornwall and South Devon. *Proceedings of the Geologists' Association, London*, **14**, 265–287, https://doi.org/10.1016/S0016-7878(63)80023-1

Dearman, W.R. 1969. On the association of upright and recumbent folds on the southern margin of the Carboniferous synclinorium of Devonshire and N. Cornwall. *Proceedings of the Ussher Society*, **2**, 115–121.

Enfield, M.A., Gilchrist, J.R., Palmer, S.N. and Whalley, J.S. 1985. Structural and sedimentary evidence for the early tectonic history of the Bude and Crackington Formations, north Cornwall and Devon. *Proceedings of the Ussher Society*, **6**, 165–172.

Ferguson, C.C. and Lloyd, G.E. 1982. Palaeostress and strain estimates from boudinage structure and their bearing on the evolution of a major Variscan fold-thrust complex in Southwest England. *Tectonophysics*, **88**, 269–289, https://doi.org/10.1016/0040-1951(82)90240-2

Finkl, C.W. and Makowski, C. 2016. *Seafloor Mapping along Continental Shelves: Research and Techniques for Visualizing Benthic Environments*. Springer, Cham, https://doi.org/10.1007/978-3-319-25121-9

Fowler, T.J. and Winsor, C.N. 1996. Evolution of chevron folds by profile shape changes: comparison between multilayer deformation experiments and folds of the Bendigo-Castlemaine goldfields, Australia. *Tectonophysics*, **258**, 125–150, https://doi.org/10.1016/0040-1951(95)00191-3

Freshney, E.C. and Taylor, R.T. 1972. The Upper Carboniferous stratigraphy of North Cornwall and West Devon. *Proceedings of the Ussher Society*, **2**, 464–471.

Freshney, E.C., McKeown, M.C. and Williams, M. 1972. *Geology of the Coast Between Tintagel and Bude*. Geological Survey of Great Britain, Memoirs, part of sheet 322 (England and Wales).

Freshney, E.C., Edmonds, E.A., Taylor, R.T. and Williams, B.J. 1979. *Geology of the Country around Bude and Bradworthy*. Geological Survey of Great Britain, Memoirs, sheets 307 and 308 (England and Wales).

Hartley, A. 1991. Debris flow and slump deposits from the Upper Carboniferous Bude Formation of SW England: implications for Bude Formation facies models. *Proceedings of the Ussher Society*, **7**, 424–426.

Hartley, A. 1993. Silesian sedimentation in south-west Britain: Sedimentation responses to the developing Variscan orogeny. *In*: Gayer, R.A., Greiling, R.O. and Vogel, A.K. (eds) *Rhenohercynian and Subvariscan Fold Belts*. Earth Evolution Series, Vieweg, Braunschweig, 159–196.

Healy, D., Rizzo, R.R. *et al*. 2017. FracPaQ: A MATLAB™ toolbox for the quantification of fracture patterns. *Journel of Structural Geology*, **95**, 1–16, https://doi.org/10.1016/j.jsg.2016.12.003

Hess, J.C. and Lippolt, H.J. 1986. $^{40}Ar/^{39}Ar$ ages of tonstein and tuff sanidines: new calibration points for the improvement of the Upper Carboniferous. *Isotope Geoscience*, **59**, 143–154, https://doi.org/10.1016/0168-9622(86)90066-7

Higgs, R. 1991. The Bude Formation (Lower Westphalian), SW England: siliclastic shelf sedimentation in a large equatorial lake. *Sedimentology*, **38**, 445–469, https://doi.org/10.1111/j.1365-3091.1991.tb00361.x

Hobson, D.M. and Sanderson, D.J. 1975. Major early folds at the southern margin of the Culm synclinorium. *Journal Geological Society of London*, **131**, 337–352, https://doi.org/10.1144/gsjgs.131.4.0337

Holloway, S. and Chadwick, R.A. 1986. The Sticklepath–Lustleigh fault zone: Tertiary sinistral reactivation of a Variscan dextral strike-slip fault. *Journal of the Geological Society, London*, **143**, 447–452, https://doi.org/10.1144/gsjgs.143.3.0447

Ji, S. and Li, L. 2020. An alternative interpretation for the formation of doubly plunging folds in sandstone terrains. *Terra Nova*, **32**, 325–333, https://doi.org/10.1111/ter.12469

Kim, Y.-S., Andrews, J.R. and Sanderson, D.J. 2001. Reactivated strike-slip faults: examples from north Cornwall. *Tectonophysics*, **340**, 173–194, https://doi.org/10.1016/S0040-1951(01)00146-9

King, A.F. 1967. *Stratigraphy and structure of the Upper Carboniferous Bude Formation, N. Cornwall*. Unpublished PhD thesis, University of Reading.

King, A.F. 1971. Correlation in the Upper Carboniferous Bude Formation, north Cornwall. *Proceedings of the Ussher Society*, **2**, 285–288.

Le Gall, B. 1990. Evidence of an imbricate crustal thrust belt in the Southern British Variscides. Contributions of SWAT deep seismic reflection profiling recorded through the English Channel and the Celtic Sea. *Tectonics*, **9**, 283–302, https://doi.org/10.1029/TC009i002p00283

Le Gall, B. 1991. Crustal evolutionary model for the Variscides of Ireland and Wales from SWAT seismic data. *Journal of the Geological Society, London*, **148**, 759–774, https://doi.org/10.1144/gsjgs.148.4.0759

Leeder, M.R. 1988. Devono-Carboniferous river systems and sediment dispersal from the orogenic belts and cratons of NW Europe. *Geological Society, London, Special Publications*, **38**, 549–558, https://doi.org/10.1144/GSL.SP.1988.038.01.37

Lloyd, G.E. and Chinnery, N. 2002. The Bude Formation, SW England – a three dimensional, intra-formational Variscan imbricate stack? *Journal of Structural Geology*, **24**, 1259–1280, https://doi.org/10.1016/S0191-8141(01)00130-4

Lloyd, G.E. and Whalley, J.S. 1986. The modification of chevron folds by simple shear: examples from North

Cornwall and Devon. *Journal Geological Society of London*, **143**, 89–94, https://doi.org/10.1144/gsjgs.143.1.0089

Lloyd, G.E. and Whalley, J.S. 1997. Simple shear modification of chevron folds: implications for facing interpretations, strain analysis and deformation history. *In*: Sengupta, S. (ed.) *Evolution of Geologic Structures from Micro to Macro Scales*. Chapman and Hall, 373–396.

Lovell, J.P.B. 1965. The Bude Sandstones from Bude to Widemouth Bay, north Cornwall. *Proceedings of the Ussher Society*, **1**, 172–174.

Macintosh, D.M. 1964. The sedimentation of the Crackington Measures. *Proceedings of the Ussher Society*, **1**, 88–89.

Mapeo, R.B.M. and Andrews, J.R. 1991. Pre-folding tectonic contraction and extension of the Bude Formation, North Cornwall. *Proceedings of the Ussher Society*, **7**, 350–355.

Melvin, J. 1986. Upper Carboniferous fine-grained turbiditic sandstones from southwest England: a model for growth in an ancient delta-fed subsea fan. *Journal of Sedimentary Petrology*, **56**, 19–34.

Nixon, C.W., Sanderson, D.J. and Bull, J.M. 2012. Analysis of a strike-slip fault network using high resolution multibeam bathymetry, offshore NW Devon UK. *Tectonophysics*, **541–543**, 69–80, https://doi.org/10.1016/j.tecto.2012.03.021

Owen, D.E. 1934. The Carboniferous rocks of the north cornish coast and their structures. *Proceedings of the Geologist's Association*, **45**, 451–471, https://doi.org/10.1016/S0016-7878(34)80019-3

Peacock, D.C.P. 2009. A review of Alpine deformation and stresses in southern England. *Italian Journal of Geosciences*, **128**, 307–316, https://doi.org/10.3301/IJG.2009.128.2.307

Ramsay, J.G. 1974. Development of chevron folds. *Geological Society of America Bulletin*, **85**, 1741–1754, https://doi.org/10.1130/0016-7606(1974)85<1741:DOCF>2.0.CO;2

Ramsbottom, W.H.C. 1969. The Namurian of Britain. *Compte Rendu du 6ème Congrès International de Stratigraphie et de Géologie du Carbonifère*, 1967, Sheffield. 71–77.

Ramsbottom, W.H.C. 1970. Some British Carboniferous goniatites of the Family Anthracoceratidae. *Bulletin Geological Survey Great Britain*, **32**, 53–60.

Ramsbottom, W.H.C. 1971. Palaeogeography and goniatite distribution in the Namurian and early Westphalian. *Compte Rendu VI Congres International Stratigraphie Carbonifere*, 1967, Sheffield. **4**, 1396–1399.

Ramsbottom, W.H.C. 1977. Major cycles of transgression (mesothems) in the Namurian. *Proceedings of the Yorkshire Geological Society*, **41**, 261–291, https://doi.org/10.1144/pygs.41.3.261

Ramsbottom, W.H.C. 1978. Distribution of British Namurian goniatites. *Compte Rendu IX Congres International Stratigraphie Carbonifere*, 1975, Moscow. **3**, 85–99.

Ramsbottom, W.H.C. 1979. Rates of transgression and regression of the Carboniferous of northwest Europe. *Journal of the Geological Society, London*, **136**, 147–153, https://doi.org/10.1144/gsjgs.136.2.0147

Ramsbottom, W.H.C., Calver, M.A., Eagar, R.M.C., Hodson, F., Holliday, D.W., Stubblefield, C.J. and Wilson, R.B. 1978. *A correlation of the Silesian rocks in the British Isles*. Geological Society of London, Special Reports, **10**.

Rattey, P.R. and Sanderson, D.J. 1982. Patterns of folding within nappes and thrust sheets – examples from the Variscan of Southwest England. *Tectonophysics*, **88**, 247–267, https://doi.org/10.1016/0040-1951(82)90239-6

Rippon, J.H. 1996. Sand-body orientation, palaeoslope analysis and basin-fill implications in the Westphalian A-C of Great Britain. *Journal of the Geological Society, London*, **153**, 881–990, https://doi.org/10.1144/gsjgs.153.6.0881

Roy, R., Launeau, P. *et al*. 2009. Geological mapping strategy using visible near-infrared–shortwave infrared hyperspectral remote sensing: application to the Oman ophiolite (Sumail Massif). *Geochemistry, Geophysics, Geosystems*, **10**, https://doi.org/10.1029/2008GC002154

Sanderson, D.J. 1974. Chevron folding in the Upper Carboniferous rocks of north Cornwall. *Proceedings of the Ussher Society*, **3**, 96–103.

Sanderson, D.J. 1979. The transition from upright to recumbent folding in the Variscan fold belt of southwest England: a model based on the kinematics of simple shear. *Journal of Structural Geology*, **1**, 171–180, https://doi.org/10.1016/0191-8141(79)90037-3

Sanderson, D.J. and Dearman, W.R. 1973.Structural styles of the Variscan fold belt in SW England, their location and development. *Journal of the Geological Society of London*, **129**, 527–536, https://doi.org/10.1144/gsjgs.129.5.0527

Saunders, W.B., Manger, W.L. and Ramsbottom, W.H.C. 1979. Donetzoceras, a mid-Carboniferous (Westphalian) index ammonoid. *Journal of Paleontology*, **53**, 1136–1144.

Selwood, E.B. and Thomas, J.M. 1985. An alternative model for the structure of north Cornwall – a statement. *Proceedings of the Ussher Society*, **6**, 180–182.

Selwood, E.B. and Thomas, J.M. 1986. Upper Palaeozoic successions and nappe structures in north Cornwall. *Journal Geological Society of London*, **145**, 75–82, https://doi.org/10.1144/gsjgs.143.1.0075

Selwood, E.B., Stewart, I.J. and Thomas, J.M.1985. Upper Palaeozoic sediments and structure in north Cornwall – a reinterpretation. *Proceedings of the Geologists Association*, **96**, 129–141, https://doi.org/10.1016/S0016-7878(85)80063-8

Tanner, P.W.G. 1989. The flexural-slip mechanism. *Journal of Structural Geology*, **11**, 635–655, https://doi.org/10.1016/0191-8141(89)90001-1

Tanner, P.W.G. 1992. Morphology and geometry of duplexes formed during flexural slip folding. *Journal of Structural Geology*, **14**, 1173–1192, https://doi.org/10.1016/0191-8141(92)90068-8

Thomas, J.H. 1988. Basin history of the Culm Trough of Southwest England. *In*: Besley, B.M. and Kelling, G. (eds) *Sedimentation in a Synorogenic Basin Complex: The Upper Carboniferous of Northwest Europe*. Blackie, Glasgow, 24–37.

Thompson, E. and Cosgrove, J.W. 1996. The structural and regional setting of the rocks of the Rusey Headland. *Proceedings of the Ussher Society*, **9**, 133–135.

Ussher, W.A.E. 1892. The British Culm Measures. *Proceedings of the Somersetshire Archaeological and Natural History Society*, **38**, 111–180.

Warr, L.N. 1989. The structural evolution of the Davidstow Anticline and its relationship to the Southern Culm Overfold, N. Cornwall. *Proceedings of the Ussher Society*, **7**, 136–140.

Warr, L.N. 2012. The Variscan Orogeny: the Welding of Pangaea. *In*: Woodcock, N. and Strachan, R.S. (eds) *Geological History of Britain and Ireland*. Wiley, https://doi.org/10.1002/9781118274064.ch15

Welker, A.J., Hogana, J.P., Eckert, A., Tindall, S. and Liu, C. 2019. Conical folds – an artefact of using simple geometric shapes to describe a complex geologic structure. *Journal of Structural Geology*, **123**, 96–104, https://doi.org/10.1016/j.jsg.2019.04.005

Whalley, J.S. and Lloyd, G.E. 1986. Tectonics of the Bude Formation, N. Cornwall: the recognition of northerly directed decollement. *Journal Geological Society of London*, **143**, 83–88, https://doi.org/10.1144/gsjgs.143.1.0083

Yeomans, C.M., Head, M. and Lindsay, J.J. 2021. Application of the tilt derivative transform to bathymetric data for structural lineament mapping. *Journal of Structural Geology*, **146**, https://doi.org/10.1016/j.jsg.2021.104301

Zwart, H.J. 1964. The development of successive structures in the Devonian and Carboniferous of Devon and Cornwall. *Geologie en Mijnbouw*, **43**, 516–526.